International Journal of Electrochemical Science 19 (2024) 100815

Contents lists available at ScienceDirect

International Journal of Electrochemical Science

journal homepage: www.editorialmanager.com/ijoes

Enhancing copper corrosion resistance in highly caustic environments: Evaluation of environmentally friendly inorganic inhibitors and mechanistic insights

Issam saber [a,*], Khadija dahmani [a], Otmane Kharbouch [b], Zakia Aribou [b], Soumya Ferraa [a], Nouf H. Alotaibi [c], Marouane El-alouani [b], Rachid Hsissou [d], Basheer M. Al-Maswari [e], Mouhsine Galai [b,*], Mohamed Ebn Touhami [b], Zaroual Aziz [b,f], M.S. El youbi [a]

[a] Laboratory of Organic Chemistry, Catalysis, and Environment, Faculty of Sciences, Ibn Tofaïl University, PO Box 133, Kenitra 14000, Morocco
[b] Laboratory of Advanced Materials and Process Engineering, Faculty of Sciences, Ibn Tofaïl University, PO Box 133, Kénitra 14000, Morocco
[c] Department of Chemistry, College of Science, King Saud University, Riyadh 11451, Saudi Arabia
[d] Laboratory of Organic Chemistry, Bioorganic and Environment, Chemistry Department, Faculty of Sciences, Chouaib Doukkali University, B.P. 20, El Jadida 24000, Morocco
[e] Department of Chemistry, Yuvaraja's College, University of Mysore, Manasagangotri, Mysuru 570 006, India
[f] Materials Laboratory Nanotechnology and Environment, Faculty of Sciences, Rabat, Morocco

ARTICLE INFO

Keywords:
Synthesis
Eco-friendly
Anticorrosion inhibitor
Copper
Sulfuric acid
Electrochemical tests

ABSTRACT

During this study, two inorganic glasses materials with chemical compositions of (1−x) ($2Bi_2O_3 \cdot B_2O_3$)–x BaO (with x=0.2 (BiB-$Ba_{0.2}$) and x=0.6 and (BiB-$Ba_{0.}6$)) were synthetized characterized and investigated as viable, ecofriendly, and sustainable inhibitors to mitigate copper corrosion in a highly caustic solution containing 0.5 M H_2SO_4 solution. To evaluate inhibition processes, several techniques were employed, including potentiodynamic polarization (PDP), electrochemical impedance spectroscopy (EIS), X-ray diffraction (XRD), Fourier transforms infrared spectroscopy (FTIR), scanning electron microscopy (SEM), energy dispersive X-ray spectroscopy (EDS), and atomic force microscopy (AFM). Furthermore, the results show that the two inhibitors studied, BiB-$Ba_{0.2}$ and BiB-$Ba_{0.6}$, have higher corrosion inhibition efficiencies at the optimum concentration (10^{-3} M), reaching 91.2 % and 90.8 %, respectively. Moreover, these findings suggest that the two inorganic compounds elaborated possess inhibitors of mixed types. Copper oxide (Cu_2O) production is markedly delayed when the two inhibitors are added to the acid medium, according to the findings of the XRD, FTIR, SEM/EDS, and AFM investigations. This outcome is explained by the development of a shield that lessens surface damage to copper metal, producing a smoother surface morphology.

1. Introduction

Corrosion represents a considerable challenge for various sectors of the economy, environment, and safety [1]. This ubiquitous problem involves the deterioration of metals due to chemical attack or environmental reactions [2], resulting in economic losses, environmental pollution, and compromised safety standards [3,4]. The complex nature of corrosion results from the interaction of multiple factors, including inherent material properties and structures, surface treatments, and environmental conditions such as chemical properties and temperature [5,6].

Copper Cu and its alloys are widely used in various fields, including electronics, civil engineering, chemical equipment, and various industrial sectors, due to their exceptional thermal and electrical conductivity, as well as their solderability [3,7]. One of the reasons for copper's widespread use is its inherent resistance to chemical and atmospheric attack, attributed to the formation of a protective film on its surface [8]. Despite this natural protection, copper remains susceptible to corrosion [9], particularly in acidic environments [10]. Acid solutions are commonly used in industrial descaling, pickling, and cleaning processes, particularly in sectors such as oil well acidification and petroleum processing [11].

* Corresponding authors.
E-mail addresses: issamsaber1993@gmail.com (I. saber), galaimouhsine@gmail.com (M. Galai).

https://doi.org/10.1016/j.ijoes.2024.100815
Received 24 August 2024; Received in revised form 27 September 2024; Accepted 27 September 2024
Available online 1 October 2024

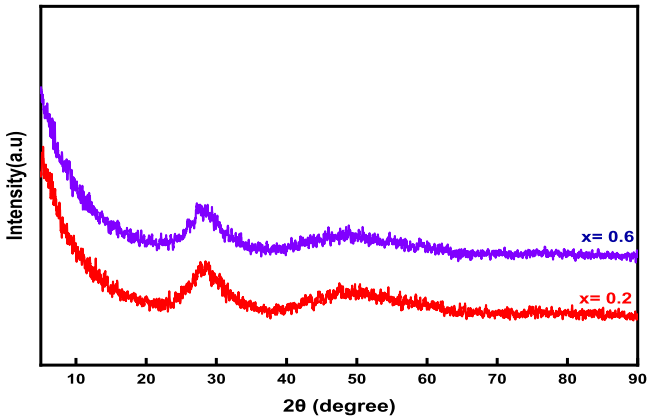

Fig. 1. X-ray diffraction of BiB-$Ba_{0.2}$ and BiB-$Ba_{0.6}$.

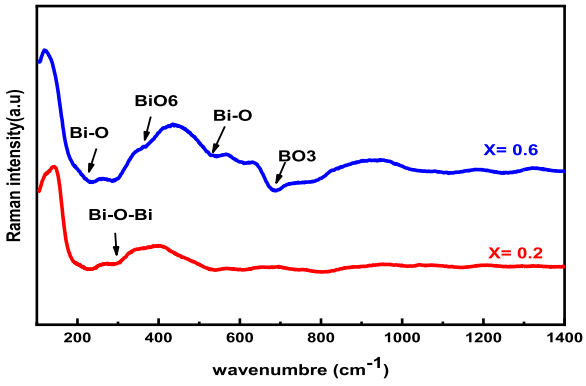

Fig. 2. Raman spectra of BiB-$Ba_{0.2}$ and BiB-$Ba_{0.6}$.

Faced with these challenges, the most effective and practical method of combating metal corrosion is to use environmentally-friendly corrosion inhibitors. These inhibitors act as a vital line of defense, reducing the impact of acid attacks on metal surfaces [12]. By using corrosion inhibitors, industries can improve the durability of metal components, reduce maintenance costs, and minimize the environmental impact associated with material degradation due to corrosion [13].

The search for environmentally friendly inhibitors is part of the wider objective of sustainable practices in industrial processes. Researchers and industry continue to explore innovative inhibitor formulations and application techniques[14–16], with the aim of striking a balance between effective corrosion protection, environmental responsibility, and economic viability [17]. The development and application of such corrosion inhibitors not only safeguards valuable assets [18], but also makes a significant contribution to preserving natural resources and reducing environmental pollution [19–21].

The use of inorganic compounds as corrosion inhibitors has been the subject of extensive research and has aroused the interest of the scientific community [22]. These inorganic corrosion inhibitors have attracted attention because of their ability to effectively mitigate corrosion. Researchers have explored a wide range of inorganic compounds for their inhibiting properties. In addition, studies have revealed that the effectiveness of these inhibitors is closely linked to the composition of the materials they are intended to protect, particularly in the context of glass-based materials [23,24]. In addition, the interaction between inorganic corrosion inhibitors and the specific composition of metal substrates plays a key role in determining inhibitor effectiveness [25]. The researchers sought to understand the complex mechanisms of adsorption, where these inhibitors bind to the surface of the substrate [26]. This adsorption process acts as a defensive countermeasure, providing a protective barrier against corrosive attack, particularly in highly acidic environments [27,28].

Exploring inorganic corrosion inhibitors and their adsorption mechanisms not only provides a better understanding of corrosion processes but also enables the development of tailor-made solutions for specific materials and environmental conditions [29]. Researchers continue to investigate new inorganic compounds and surface interactions with the aim of improving the effectiveness of corrosion inhibition methods [30].

In this prospective study, the utilization of two inorganic glasses materials with chemical compositions of (1−x) (2Bi_2 O_3 ·B_2 O_3)–x BaO (with x=0.2 (BiB-$Ba_{0.2}$) and x=0.6 and (BiB-$Ba_{0.}$6)) outstanding results in terms of corrosion protection for copper electrodes in 0.5 M H_2SO_4 solution. Various techniques, such as EIS, PDP, XRD, FTIR, AFM, and SEM/EDS, were employed to assess the inhibition processes comprehensively. Moreover, the novelty of this research prompted an in-depth exploration to comprehend the inhibition mechanism between the tested synthesizes glasses and copper substrates. These substances demonstrated their ability to prevent copper corrosion effectively by safeguarding metal substrates through adsorption mechanisms, thereby delaying the onset of metal corrosion.

2. Experimental procedure

2.1. Glass synthesis

Two inorganic glasses materials investigated in this potential study were synthesized with chemical compositions of (1−x) (2Bi_2 O_3 ·B_2 O_3)–x BaO (with x=0.2 (BiB-$Ba_{0.2}$) and x=0.6 and (BiB-$Ba_{0.}$6)). These materials were prepared using stoichiometric mixtures of chemically pure reagents, including the commercial oxides H_3BO_3 (Aldrich), Bi_2O_3 (Fulka), and $BaCO_3$ (Riedel-de-Haën).

The synthesis process is as follows.

$$(1-x)(2Bi_2O_3 + H_3BO) + xBaCO_3 \xrightarrow{400^\circ C} (1-x)(2Bi_2O_3.B_2O_3) + xBaO + CO_2 + H_2O$$

Initially, the raw materials are ground in an agate mortar to achieve homogeneity. Subsequently, the mixture is melted in alumina crucibles at 450 °C for 12 hours to eliminate any organic matter. After each reaction, the resulting mixture is ground again to ensure homogeneity and then subjected to a gradual heat treatment at 1000 °C for 1 h [31].

2.2. Glass characterization

In the present study, the glassy compounds studied were characterized using various analytical methods, namely XRD, Raman, FTIR, and SEM.

2.2.1. XRD analysis

The X-ray diffraction spectrum of the prepared glass samples were recorded at room temperature, as shown in Fig. 1. This clearly demonstrates the amorphous nature of the glass samples investigated.

2.2.2. Raman analysis

Raman analysis was conducted on the compounds tested in the range of 100–1400 cm-1 at room temperature to identify the local structure of the glass system (Fig. 2).

The Raman spectra of the test glasses were analyzed in the frequency range of 100–1400 cm^{-1} and are presented in Fig. 2. The figure illustrates the molecular vibrations, crystal lattice vibrational modes, and band positions at 120–140 cm^{-1}, 265 cm^{-1}, 340 cm^{-1}, 390–450 cm^{-1}, 560–640 cm^{-1}, 690 cm^{-1}, 720 cm^{-1}, and 916 cm^{-1}[32–34]

2.2.3. FTIR characterization

Fig. 3 displays the infrared absorption spectra (FTIR) of the studied glasses, which were recorded in the range from 400 to 2000 cm^{-1} at

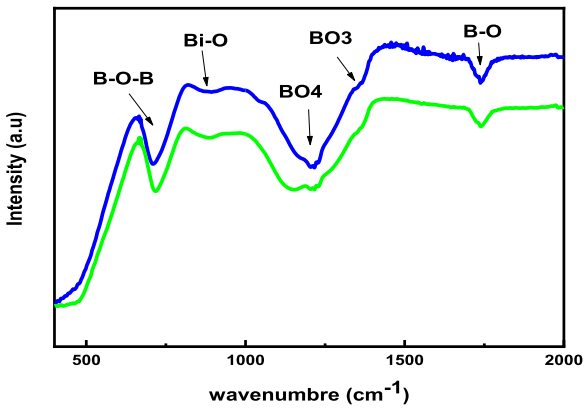

Fig. 3. FTIR spectra of BiB-$Ba_{0.2}$ and BiB-$Ba_{0.6}$.

room temperature. This analysis was conducted to examine the vibrational modes and fully identify the local structure of the glass system [35–37].

2.2.4. SEM study

The surface morphology of the studied inorganic compounds was examined and evaluated using scanning electron microscopy. Fig. 4 presents SEM images of the inhibitors tested with varying BaO contents. It was observed that the grains formed on the surface of the different glasses were not homogeneous. Additionally, the surface images revealed variations in grain size across all compounds, with an increase in grain size corresponding to higher BaO content[31].

2.3. Preparation of the electrode and the solution

For the present study, metallic copper was used predominantly for all tests, with chemical compositions distributed as shown in Table 1:

Moreover, copper is the predominant element at 99.936 %, and the other elements are considered impurities in this metal.

The 1 cm^2 copper metal surfaces selected for the electrochemical tests were prepared through mechanical polishing using progressively finer grit sandpaper, ranging from 220 to 2000, to achieve varying degrees of flatness and roughness. Subsequently, the surfaces were thoroughly rinsed and degreased with distilled water and acetone. Finally, they were left to air-dry at room temperature.

Furthermore, all electrochemical studies were conducted in a corrosive environment containing 0.5 M H_2SO_4. This solution was prepared by diluting analytical grade H_2SO_4 (98 % by weight) with distilled water. Simultaneously, corrosion tests were conducted in an acidic environment both without and after the addition of varying concentrations of the two new inorganic inhibitors BiB-$Ba_{0.2}$ and BiB-$Ba_{0.6}$, ranging from 10^{-3} to 10^{-6} M.

2.4. Electrochemical measurement

In the present study, electrochemical studies were conducted using a measuring apparatus comprising three electrodes: a copper plate employed as the working electrode, a platinum rod serving as the counter electrode, and a saturated calomel electrode (SCE) used as the reference electrode [38].

Electrochemical measurements were performed using a PGZ100 Potentiostat/Galvanostat connected to a computer and controlled by analysis software (Volta Master 4). The polarization curves (PDP traces) were recorded while varying the potential from −1200–300 mV, with a scan speed of 1 mV/s, at room temperature (T = 298 K). Copper samples were immersed in a 0.5 M H_2SO_4 acid solution during treatment with different concentrations of inhibitors BiB-$Ba_{0.2}$ and BiB-$Ba_{0.6}$, data analysis involved fitting Tafel polarization curves and processing EIS data using EC-Lab V10.02 software, where the corrosion current density (Icorr) and other electrochemical parameters (E_{corr}, cathodic and anodic Tafel slopes (βc and βa) were extracted by selecting a range of ±100 mV around the corrosion potential (Ecorr), with 100 mV in the anodic region and 100 mV in the cathodic region. Additionally, the inhibition performance (η) was calculated as Eq. 1 follows [39]

$$\eta = \left(\frac{i^{\circ}_{corr} - i_{corr}}{i^{\circ}_{corr}} \right) \times 100\% \quad (1)$$

The electrochemical impedance spectroscopy (EIS) tests were conducted using an alternating current (AC) signal of 10 mV in the

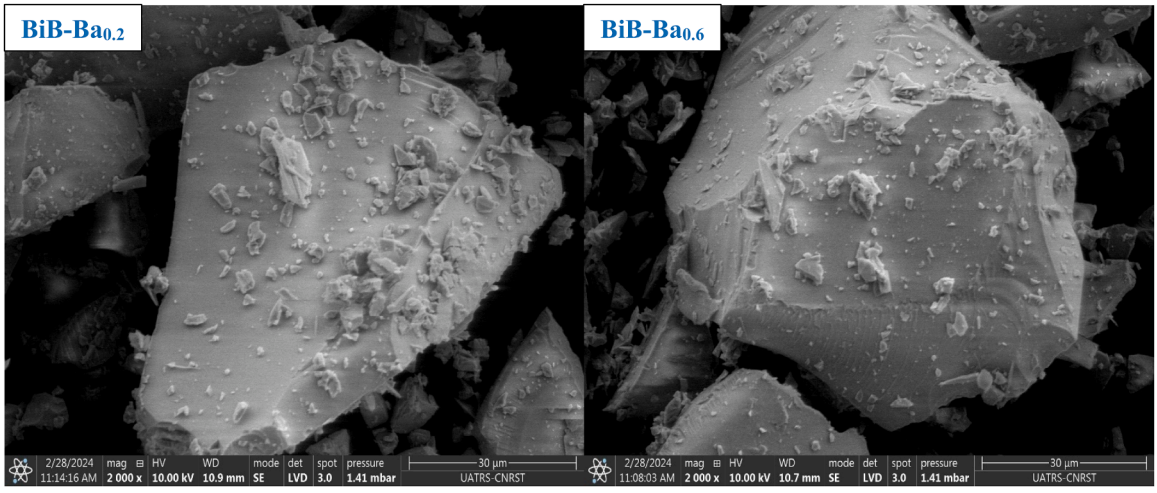

Fig. 4. SEM micrograph of preparedBiB-$Ba_{0.2}$ and BiB-$Ba_{0.6}$ glasses.

Table 1
The chemical composition of the tested copper samples.

Elements	C	P	Fe	As	Pb	Mn	Sb	Bi	Al	Ni	Ag	Sn	S	Cu
Chemical Composition (%)	0.005	0.019	0.001	0.001	0.015	0.001	0.002	0.001	0.001	0.003	0.005	0.009	0.001	99.936

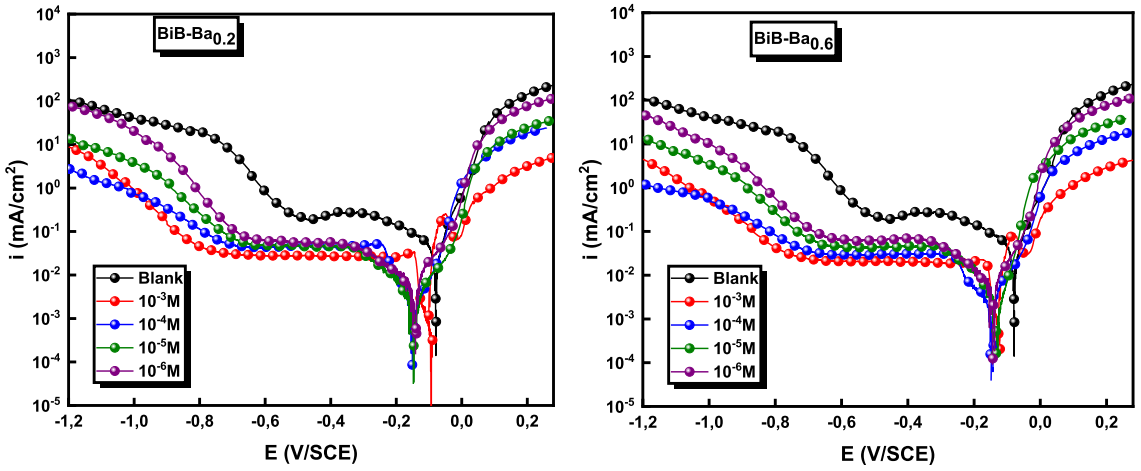

Fig. 5. Stationary polarization conduits for copper corrosion in 0.5 M H_2SO_4 without and with different concentrations of BiB-$Ba_{0.2}$ and BiB-$Ba_{0.6}$.

frequency range of 100 KHz to 1 mHz. Copper was immersed in a corrosive solution of 0.5 M H_2SO_4 for 30 minutes with the addition of various concentrations of BiB-$Ba_{0.2}$ and BiB-$Ba_{0.6}$, as well as in the absence of these concentrations. The EIS parameters were determined using an equivalent electrical circuit. The corrosion efficiencies (η) for EIS were measured using the follows Eq. 2.

$$\eta = \left(1 - \frac{R_P^{\circ}}{R_P} \right) \times 100\% \quad (2)$$

2.5. Surface characterization

2.5.1. X-ray diffraction analysis

The XRD technique was employed on copper substrates immersed for 12 hours in a more aggressive medium containing 0.5 M H_2SO_4, both before and after exposure to an optimal concentration (10^{-3} M) of two inhibitors tested, BiB-$Ba_{0.2}$ and BiB-$Ba_{0.6}$. These analyses were conducted using an X-ray diffractometer (Panalytical's X'Pert^3) with a Cu Kα radiation source as the target (λ = 1.5406 Å).

2.5.2. FTIR analysis

In order to better treat the copper surface, an infrared spectroscopy analysis (BRUKER TENSOR II) was carried out between the region of 400 and 2000 cm^{-1} at room temperature. FT-IR measurements were carried out after 12 hours immersion in an aggressive medium examined before and after exposure to an optimum concentration (10^{-3} M) of the two inhibitors tested BiB-$Ba_{0.2}$ and BiB-$Ba_{0.6}$.

2.5.3. SEM/EDS and AFM study

Energy dispersive X-ray spectroscopy and scanning electron microscopy were used to analyses the surface morphology and chemical composition of copper samples that had been immersed in an aggressive environment containing 0.5 M H_2SO_4 for 12 hours. These samples were examined before and after exposure to an optimal concentration of two inhibitors (10^{-3} M). Using atomic force microscopy (AFM) and a Bruker Veeco Dimension ICON, the morphology of the deposited films was investigated at room temperature. Using a molecular imaging system with a silicon nitride cantilever, AFM imaging was carried out in tapping mode, allowing for a thorough surface investigation.

3. Results and discussion

3.1. Effect of inhibitor concentration

3.1.1. Potentiodynamique polarization curves

To explore the interaction mechanisms between the inhibiting inorganic compound tests and copper surface samples, both uninhibited and inhibited with these substances at different concentrations in 0.5 M H_2SO_4 at 298 K, the study employed potentiodynamic polarization curves, as depicted in Fig. 5. This analytical approach is essential for understanding the electrochemical behavior of the copper surface under various conditions.

The following Eqs. 3 and 4 describe the anodic copper corrosion process and the cathodic oxygen reduction reaction in a medium containing 0.5 M H_2SO_4, respectively. The anodic mechanism process is described as follows [40]

$$Cu \rightarrow Cu^{+} + e^{-} \quad (3)$$

$$Cu^{+}_{ads} \rightarrow Cu^{2+} + e^{-} \quad (4)$$

The mechanism of the cathodic process is described as Eq. 5 follows [41]

$$\frac{1}{2}O_2 + 2H^{+} + 2e^{-} \rightarrow H_2O \quad (5)$$

From the reaction mechanism (Eqs. 3 and 4), it is clear that the copper electrode allows the generation of Cu^{2+} ions inside a solution of sulfuric acid and air. The inhibitor molecule, therefore, most probably reacts with the Cu^{2+} ion to adsorb onto the Cu surface. The interaction mechanism is expressed by the Eq. 6 following:

$$Cc^{+}_{ads} + nInh \rightarrow [Cu - InH_n]^{n}_{ads} \quad (6)$$

From the variations in the cathodic and anodic branches for all the inhibitors studied, it can be concluded that the cathode (oxygen reduction) and the anode reaction mechanisms are the same for all inhibitors of BiB-$Ba_{0.2}$ and BiB-$Ba_{0.6}$.

The data presented in Fig. 5 shows a clear trend. As the concentrations of the two inhibiting substances increased progressively (from 10^{-6} to 10^{-3} M), the corrosion potential (ΔE_{corr}) shifted negatively. This change suggests a move towards a more electronegative potential, indicating the inhibitory effect of these substances on the corrosion process of copper in an acidic environment [42].

Additionally, the corrosion current density decreased significantly in the presence of the inhibitors compared to the blank solution of copper samples. The decrease in i_{corr} indicates that the inhibitors form a protective layer on the surface of the copper, hindering the corrosion process. This suggests the creation of an adsorption barrier by the tested inhibitors onto the copper surface, which reduces the corrosion current density and signifies a lower rate of corrosion [43]. Furthermore, the cathodic curves prior to and in the presence of BiB-$Ba_{0.2}$ and BiB-$Ba_{0.6}$ are nearly indistinguishable, indicating that these compounds do not modify the reaction mechanism of the cathode [44]

Table 2
PDP parameters for copper corrosion in 0.5 M H_2SO_4 with and without BiB-$Ba_{0.2}$ and BiB-$Ba_{0.6}$.

inhibitor	Conc (M)	$-E_{corr}$ (mV/ SCE)	i_{corr} ($\mu A\ cm^{-2}$)	$-\beta_c$ ($mV\ dec^{-1}$)	β_a ($mV\ dec^{-1}$)	η %
Blank	–	79	29.0	204	59	-
BiB-$Ba_{0.2}$	10^{-3}	84	2.5	174	54	91.2
	10^{-4}	144	2.9	162	53	89.7
	10^{-5}	119	3.0	179	51	89.6
	10^{-6}	134	6.2	176	49	78.3
BiB-$Ba_{0.6}$	10^{-3}	114	2,6	187	58	90.8
	10^{-4}	141	3.0	189	56	89.5
	10^{-5}	131	3.3	165	53	88.4
	10^{-6}	143	8.9	173	51	69.1

The formation of the adsorption barrier is crucial. It indicates that the inhibiting compounds attach effectively to the copper surface, creating a protective layer that shields the metal from the corrosive attack of the sulfuric acid solution. This barrier acts as a deterrent, limiting the interaction between the copper surface and the corrosive environment. Consequently, this inhibits electrochemical reactions that lead to corrosion, enhancing the overall corrosion resistance of the copper material [45].

The passive current density, i_pass, for the copper alloy can be derived from the plateau region in the anodic polarization curve where the current density stabilizes. In Fig. 5, this occurs between the potentials of approximately 0 V to 0.2 V vs SCE for both BiB-Ba0.2 and BiB-$Ba_{0.6}$ at different concentrations, in both the BiB-Ba0.2 and BiB-Ba0.6 inhibitors, it is clear that as the concentration of the inhibitor increases from 10^{-6} M to 10^{-3} M, the passive current density decreases significantly. This means that the copper corrosion is being effectively suppressed by the inhibitor at higher concentrations, as the concentration increases (10^{-3} M), the passive current density decreases significantly, indicating that the inhibitor is forming a more protective and stable passive layer on the copper surface. This protective layer prevents active corrosion processes, leading to a more passive behavior.

Table 2 presents a comprehensive overview of the PDP parameters.

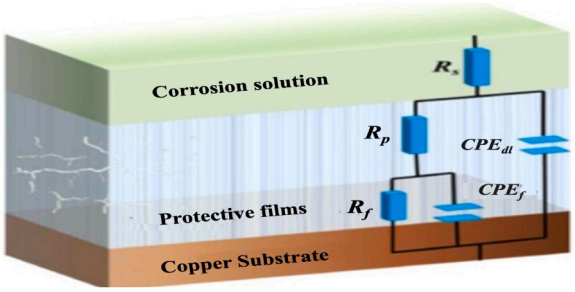

Fig. 8. Equivalent circuit schemes for BiB-$Ba_{0.2}$ and BiB-$Ba_{0.6}$ in 0.5 M H_2SO_4 for EIS data adjustment.

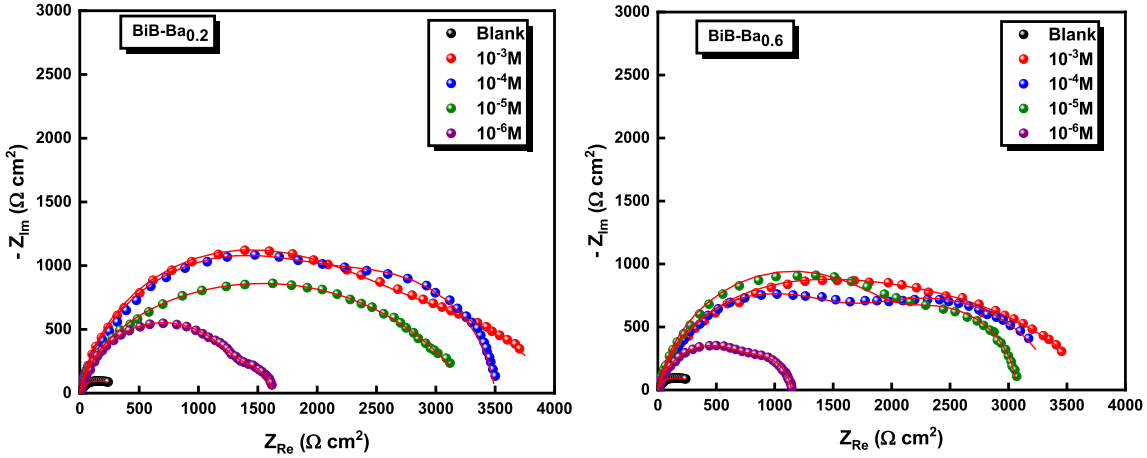

Fig. 6. Nyquist curves for copper in 0.5 M H_2SO_4 without and with different concentrations of BiB-$Ba_{0.2}$ and BiB-$Ba_{0.6}$.

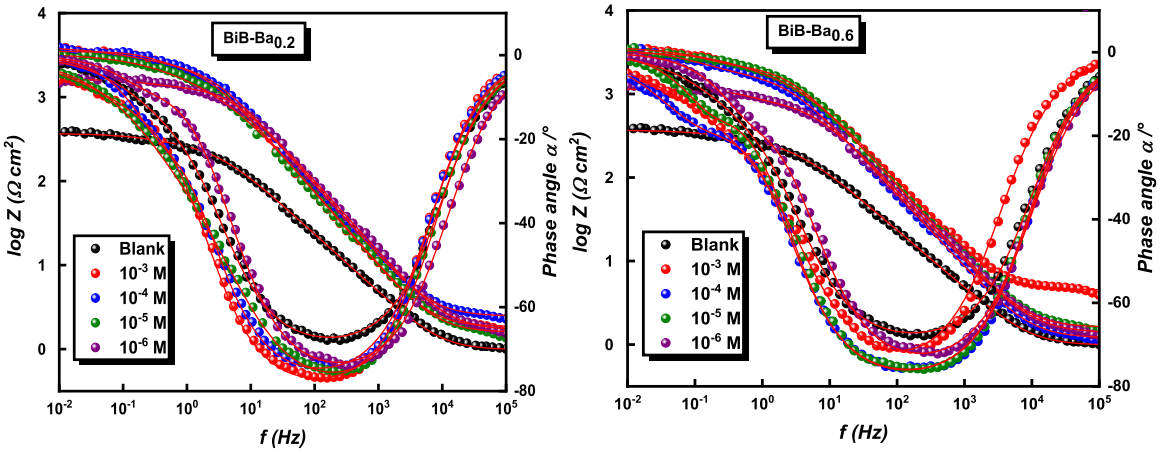

Fig. 7. Bode-phase curves for copper in 0.5 M H_2SO_4 without and with different concentrations of BiB-$Ba_{0.2}$ and BiB-$Ba_{0.6}$.

Table 3
EIS parameters for copper corrosion in 0.5 M H_2SO_4 without and with of BiB-$Ba_{0.2}$ and BiB-$Ba_{0.6}$.

Inhibitors	*Conc. (M)*	R_s (Ωcm^2)	CPE_f (μFcm^2)	n_f	R_f (Ωcm^2)	CPE_{dl} (μFcm^2)	n_{ct}	R_{ct} (Ωcm^2)	R_p (Ωcm^2)	θ	η (%)
Blank	–	0.7	-	-	-	475	0.720	350	350	–	-
BiB-$Ba_{0.2}$	10^{-3}	1.8	39.9	0.888	2 464	125	0.603	1 557	4 021	0.912	91.2
	10^{-4}	2.4	40.8	0.865	2 608	179	0.996	889	3 497	0.899	89.9
	10^{-5}	1.5	43.6	0.885	2 259	251	0.655	1 049	3 308	0.894	89.4
	10^{-6}	1.6	47.1	0.855	1 386	315	0.945	237	1 623	0.784	78.4
BiB-$Ba_{0.6}$	10^{-3}	4.4	43.0	0.858	2 254	106	0.615	1 564	3 818	0.908	90.8
	10^{-4}	1.1	43.3	0.876	1 756	107	0.753	1 669	3 425	0.897	89.7
	10^{-5}	1.5	56.7	0.878	2 270	125	0.768	800	3 070	0.885	88.5
	10^{-6}	1.3	60.1	0.849	884	405	0.547	257	1 141	0.693	69.3

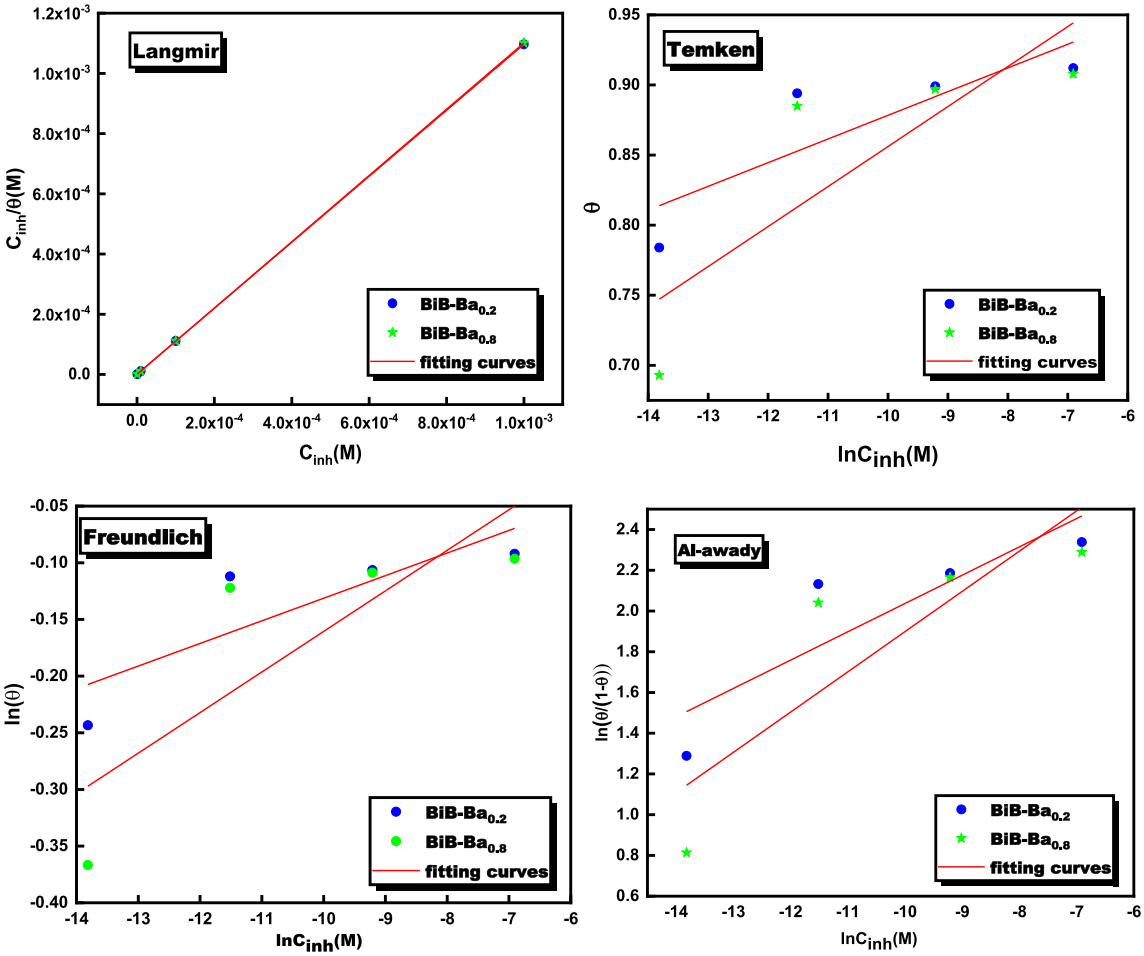

Fig. 9. Plots of the various adsorption isotherms for products of BiB-$Ba_{0.2}$ and BiB-$Ba_{0.6}$ tested on the copper surface in 0.5 M H_2SO_4 at 298 K.

Table 4
Correlation coefficients of the isotherms of the adsorption models.

	compounds	Langmuir	Temkin	Freundlich	Al-awady
R^2	BiB-$Ba_{0.2}$	1	0.7167	0.7093	0.7639
	BiB-$Ba_{0.6}$	1	0.6879	0.6778	0.7397

Table 5
Adsorption parameters for BiB-$Ba_{0.2}$ and BiB-$Ba_{0.6}$ inhibitors on copper substrates.

compound	K_{ads} (L / mol)	$-\Delta G_{ads}$ (kJ/mol)	R^2
BiB-$Ba_{0.2}$	153.6 10^4	45.2	1
BiB-$Ba_{0.6}$	152.1 10^4	45.1	1

One of the main observations is the progressive decrease in i_{corr} with increasing inhibitor concentration, ranging from 10^{-6} to 10^{-3} M. The decreasing values of i_{corr} indicate a reduction in the metal's susceptibility to corrosion, demonstrating the inhibitors' effectiveness in hindering the electrochemical reactions responsible for corrosion. Furthermore, the observed shift of E_{corr} towards the negative direction in comparison to the blank solution is a significant finding [46]. The shift of less than 85 mV indicates that the copper electrode's surface tends to corrode at more electronegative potentials in the presence of inhibitors. This shift towards the negative zone suggests that the inhibitors have a mixed nature, meaning they can both dissolve the metal and reduce the

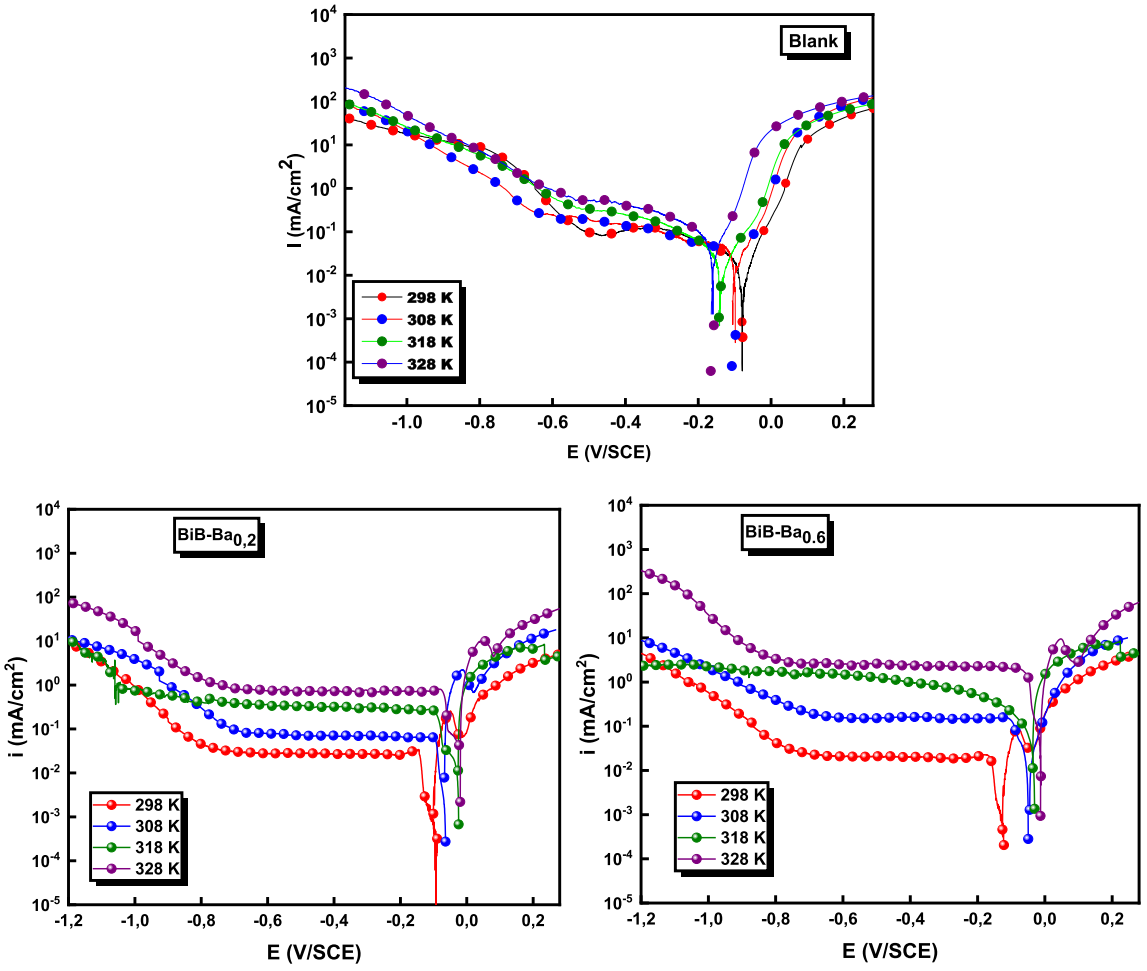

Fig. 10. Corrosion polarization curves for copper in 0.5 M H_2SO_4 without and with inhibitors at different temperatures.

Table 6
Activation parameters of BiB-$Ba_{0.2}$ and BiB-$Ba_{0.6}$ inhibitors for Cu corrosion in a 0.5 M H_2SO_4 acid medium at various temperatures.

Compound	*Temperature* (K)	*-E_{corr} (mV/ SCE)*	*i_{corr} ($\mu A/cm^2$)*	*-β_c (mV. dec^{-1})*	*β_a (mV. dec^{-1})*	*η (%)*
Blank	298	79	29.0	204	59	-
	308	105	35.0	188	54	-
	318	142	56.0	164	52	-
	328	166	77.0	152	51	-
BiB-$Ba_{0.2}$	298	84	2.5	174	54	91.2
	308	60	3.6	158	51	89.7
	318	19	6.8	164	49	87.8
	328	23	10.4	153	47	86.4
BiB-$Ba_{0.6}$	298	114	2.6	187	55	90.8
	308	32	3.7	185	53	89.4
	318	17	7.0	158	52	87.5
	328	3	11.0	154	49	85.7

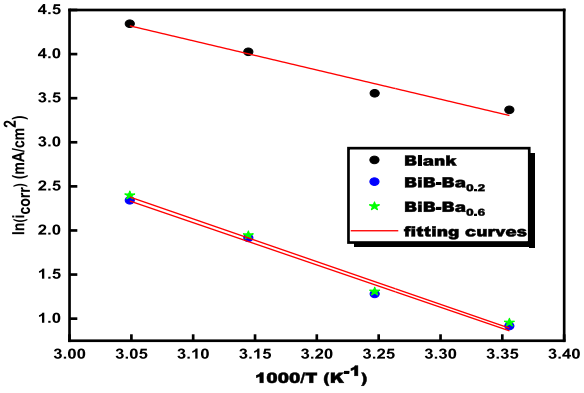

Fig. 11. Arrhenius diagrams for copper samples in 0.5 M H_2SO_4 without and with BiB-$Ba_{0.2}$ and BiB-$Ba_{0.6}$ inhibitors at different temperatures.

corrosive species. This dual-action mechanism improves the overall effectiveness of inhibitors, making them versatile in protecting the copper surface against corrosion [47].

Upon closer examination of the results presented in Table 2, it is clear that the βc slopes are slightly modified when inorganic inhibitors are introduced into the aggressive environment. The inhibitory efficiency increases significantly, reaching high percentages of 91.2 % for BiB-$Ba_{0.2}$ and 90.8 % for BiB-$Ba_{0.6}$ at the maximum concentration. The increase in inhibitory efficiency strongly suggests that these compounds may be adsorbed onto the surface of the copper electrode, particularly as their concentration increases. This phenomenon indicates a more significant interaction between the inhibitors and the copper surface, further supporting the effectiveness of these inorganic compounds in inhibiting the corrosion process.

3.1.2. EIS measurements

The electrochemical impedance spectroscopy (EIS) technique provides explanations of the dynamics and structure of the surface of copper

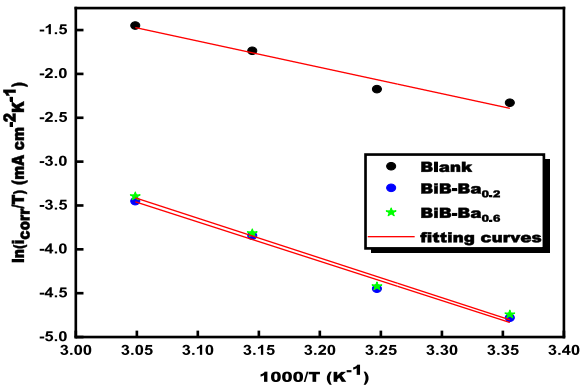

Fig. 12. Transition state diagrams for copper samples in 0.5 M H_2SO_4 without and with of BiB-$Ba_{0.2}$ and BiB-$Ba_{0.6}$ inhibitors at different temperatures.

Table 7
Kinetic activation parameters for copper substrate in blank without and addition of the BiB-$Ba_{0.2}$ and BiB-$Ba_{0.6}$.

Compound	molar Mass(g/mol)	E_a (kJ mol^{-1})	ΔH_a (kJ mol^{-1})	ΔS_a (J mol^{-1} K^{-1})
Blank	——	27.5	25.0	−134.0
BiB-$Ba_{0.2}$	831.8972	39.8	37.2	−112.7
BiB-$Ba_{0.6}$	492.6116	40.2	37.6	−111.1

metal used as the working electrode. EIS has been widely employed in the field of metal corrosion protection. Fig. 6 displays Nyquist diagrams for copper in the 0.5 M H_2SO_4 environment, both uninhibited and inhibited with different concentrations of BiB-$Ba_{0.2}$ and BiB-$Ba_{0.6}$ at 298 K.

Nyquist plots provide valuable insights into the electrochemical aspects of the system being studied, enhancing our understanding of the protective mechanisms involved. The presence of semicircles, coupled with flattened capacitance loops, indicates the frequency dispersion of the interfacial impedance. As shown in Fig. 6, it is evident that the charge transfer impedance and the diameter of the half-loops increase with the addition of varying concentrations of BiB-$Ba_{0.2}$ and BiB-$Ba_{0.6}$ to the blank solution. This trend suggests that these compounds are adsorbed onto copper surfaces, forming a protective layer that effectively inhibits metal dissolution.

Moreover, the presence of a second capacitive loop in all low-frequency experiments indicates the existence of adsorbed species on the electrode surface. The first loop, observed at low frequencies, can be attributed to the combination of double-layer capacitance and charge-transfer resistance. In contrast, the appearance of the second loop at high frequencies indicates the successful and efficient adsorption of the inhibitor molecules onto the Cu surface. This dual-loop behavior highlights the complex interplay between electrochemical processes and underscores the effectiveness of the adsorbed species in forming a protective barrier on the Cu surface. This enhances our understanding of the underlying protective mechanisms [48].

The data presented in Fig. 7 offer important insights into the inhibition capabilities of the inorganic substances examined. The Bode traces clearly show a significant increase in the phase angle and impedance modulus at low frequencies in all the experiments carried out in the presence of the two inhibiting molecules, BiB-$Ba_{0.2}$ and BiB-$Ba_{0.6}$. This remarkable improvement signifies the ability of these substances to form a highly effective adsorption barrier on the active sites of the working electrode surface, effectively preventing copper corrosion. In addition, the observed increase in the low-frequency impedance modulus, as indicated by the Bode diagrams, implies that an increase in the concentration of these molecules leads to an improvement in the

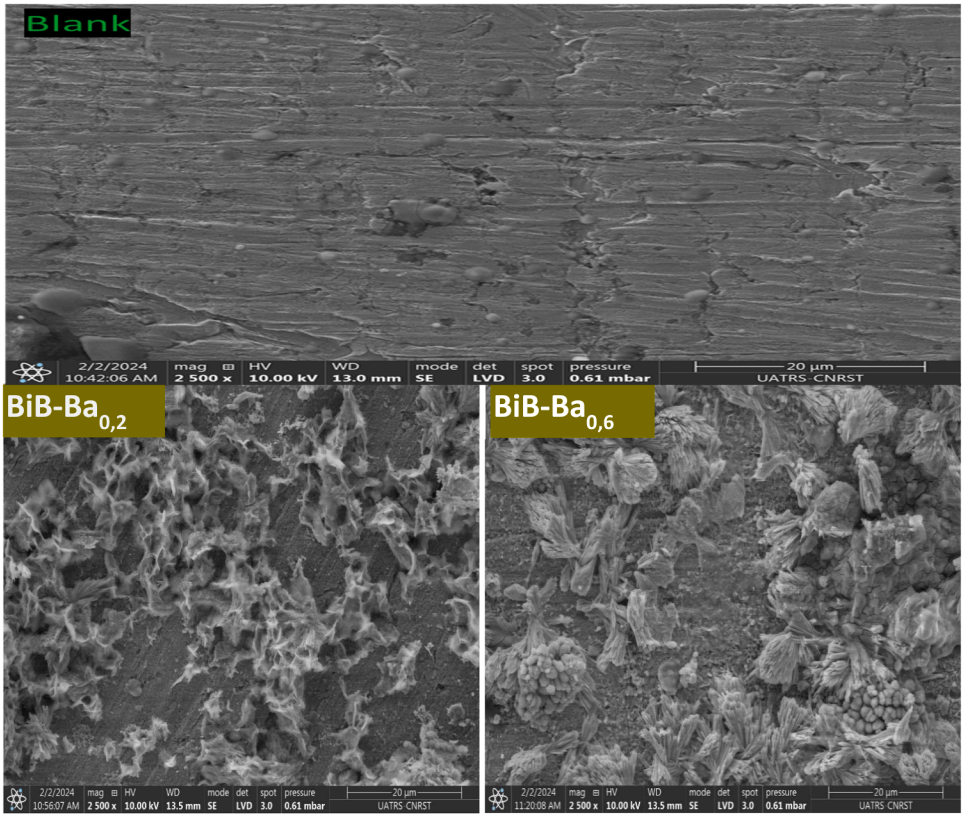

Fig. 13. SEM images of copper substrates immersed in a corrosive medium without and with the addition of BiB-$Ba_{0.2}$ and BiB-$Ba_{0.6}$ inhibitors at 10^{-3} M for 12 hours.

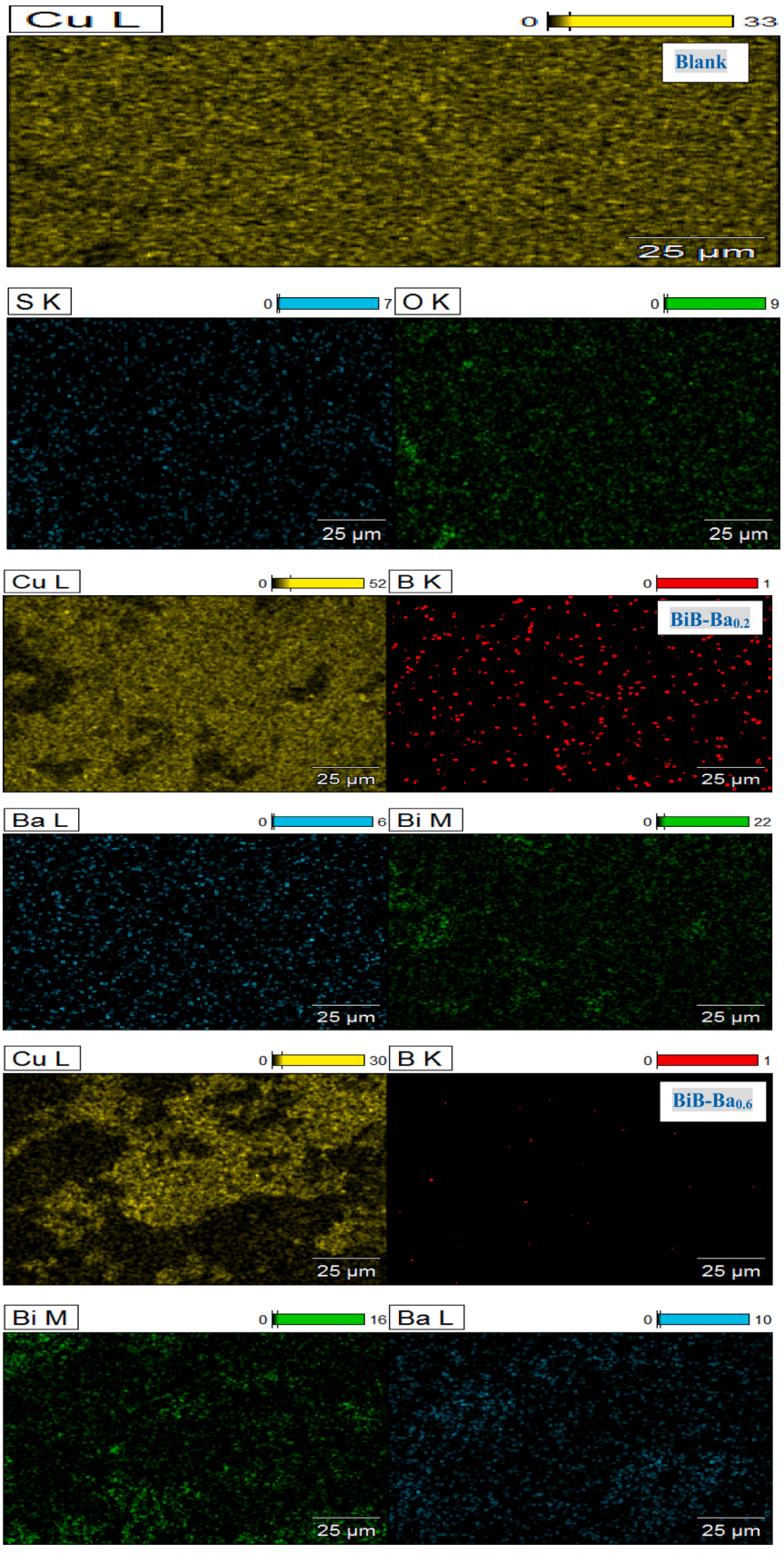

Fig. 14. EDS elemental mapping of copper, oxygen, Bi, B, Ba, and S atoms on copper substrates immersed in a corrosive medium without and with the addition of inhibitors.

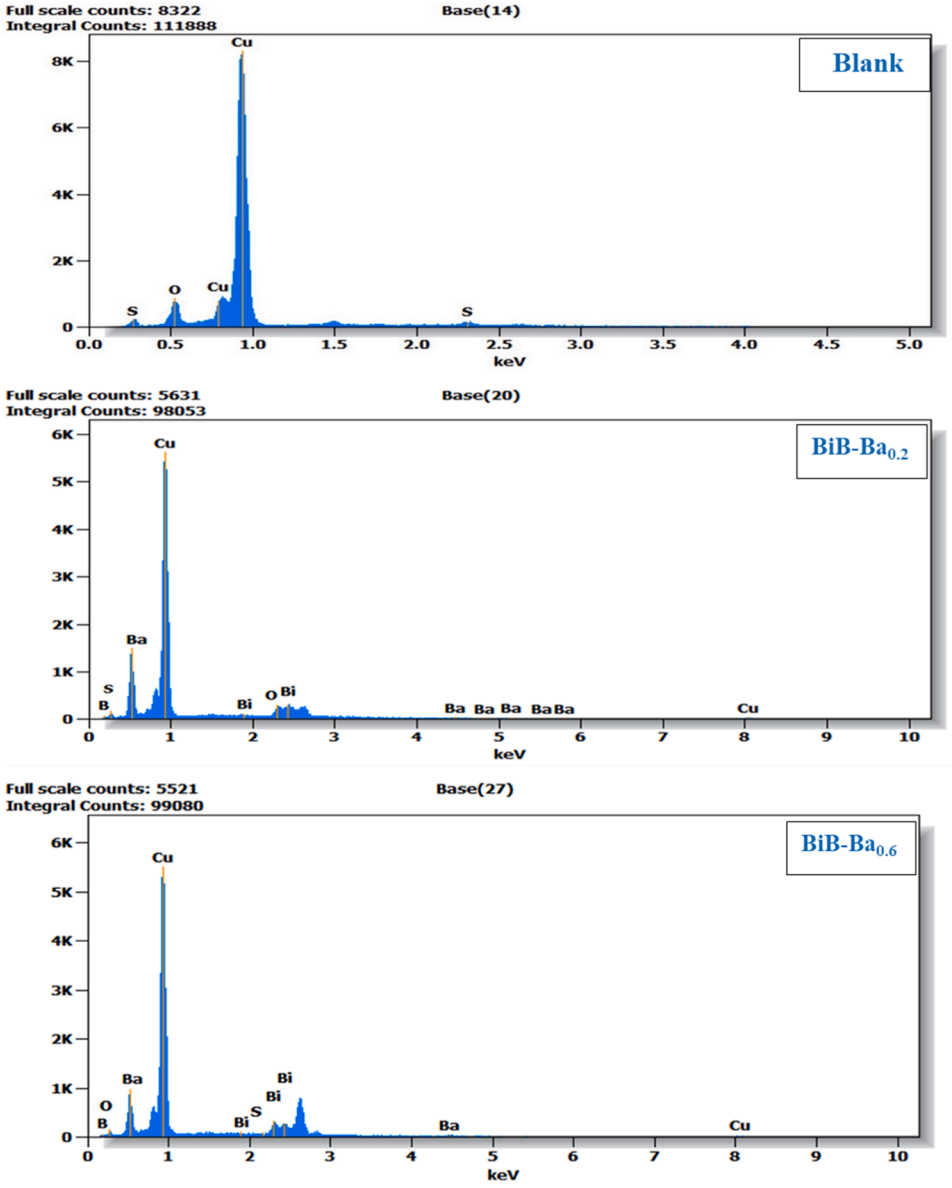

Fig. 15. EDS spectra obtained by immersing copper substrates for 12 hours in a corrosive medium before and after addition of the inhibitors BiB-$Ba_{0.2}$ and BiB-$Ba_{0.6}$ at 10^{-3} M.

Table 8
Different percentages of the elements constituting glass compounds.

Compounds	O (%)	S (%)	Cu (%)	Bi (%)	B (%)	Ba (%)
Blank	11.9	2.5	85.6	—	—	—
BiB-$Ba_{0.2}$	1.6	1.0	86.6	4.1	1.4	5.3
BiB-$Ba_{0.6}$	1.2	1.1	87.0	3.4	2.6	4.7

performance of the inhibitor's protective layer [49]. This concentration-dependent effect suggests that higher concentrations of inhibitor molecules result in a stronger and more durable protective layer, further enhancing their anti-corrosion properties [50].

Fig. 8 shows the equivalent electrical circuits used to fit the experimental EIS and Bode data. The language used is clear, concise, and objective, with technical terms explained when first used. The text adheres to conventional academic structure and formatting, with consistent citation and footnote style [51]. The circuit include important elements such as the solution resistance (R_s), the polarization resistance (R_p) which contains charge transfer resistance (R_{ct}), diffuse layer resistance (R_d), and the resistance accumulated species such as corrosion products, any existing molecules or ions. R_f represents the film resistance. Also, $R_{sum} = R_p + R_f$ [52]. Additionally, the constant phase elements (CPE) are labeled CPE_{dl} and CPE_f [53]. These elements characterize the non-ideal behavior of the system. CPE_f represents the constant phase element associated with the oxide film, capturing its impedance properties. CPE_{dl} represents the constant phase element associated with polarization resistance, accounting for the electrical behavior at the electrode-electrolyte interface [54].

However, the CPE was used to adjust the Nyquist curves to take into account inhomogeneity and other factors such as impurities and adsorption spices on the copper surface. The impedance of the CPE (Z_{CPE}) value was determined by the Eq. 7 [55,56]

$$Z_{CPE} = \frac{1}{Y_0(j\omega)^n} \tag{7}$$

Where j presents the imaginary indice, ω presents the angular frequency, Y_0 represents the CPE coefficient, and n indicates the deviation parameter related to the phase deviation.

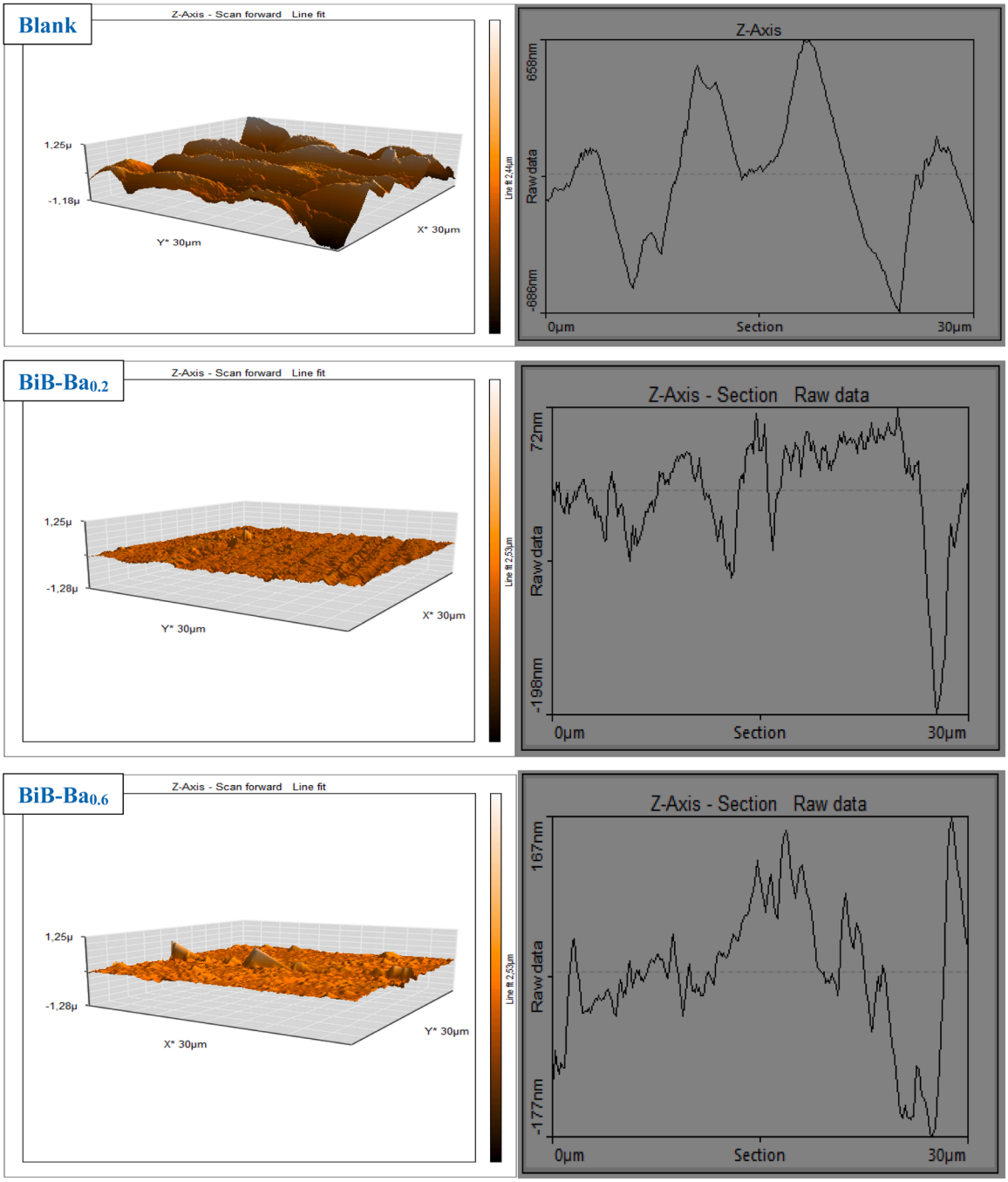

Fig. 16. 3D AFM images and raw data of the copper electrode after immersion in a 0.5 M H_2SO_4 solution in the absence and presence of 10^{-3} M of the two inorganic compounds studied.

The values for C_{dl} and film capacitance C_f can be calculated using the Eq. 8 following [57,58]

$$C = Y_0(\omega)^{n-1} = Y(2\pi f z_{im-Max})^{n-1} \quad (8)$$

Where the f Z_{im} - Max term presents the frequency at which the imaginary part reaches its maximum in the EIS curves.

Polarization resistance values (R_p) were obtained according to the Eq. 9 given below:

$$R_P = R_f + R_{ct} + R_s \quad (9)$$

Table 3 presents the results, which show a clear trend: as the concentration of the two compounds in the blank solution increases, the values of R_{ct}, R_f, and corrosion efficiency gradually rise. This indicates that the tested compounds have a significant impact on inhibiting the copper corrosion process. Furthermore, the decrease in CPE_{dl} and CPE_f as the compound concentration increases suggests that these compounds adhere to the Cu surface, hindering the charge transfer reactions that are involved in the corrosion process. It can be inferred that the corrosion efficiency reaches 91.2 % for the compound of BiB-$Ba_{0.2}$ when present at a concentration of 10^{-3} M in the aggressive medium under study.

3.2. Adsorption isotherm

Adsorption isotherms are another essential approach to understanding the corrosion process and inhibition mechanisms. Moreover, the correlation coefficient (R^2) was considered the best fit to the

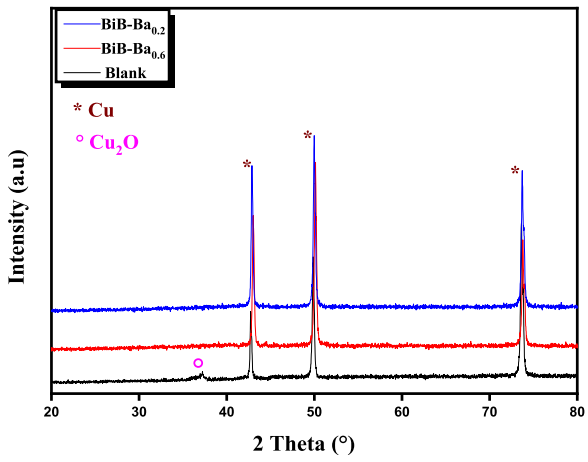

Fig. 17. XRD patterns of copper substrates immersed for 12 h in a corrosive acid (H_2SO_4 0.5 M) alone and after addition of inhibitors of BiB-$Ba_{0.2}$ and BiB-$Ba_{0.6}$ at 10^{-3} M.

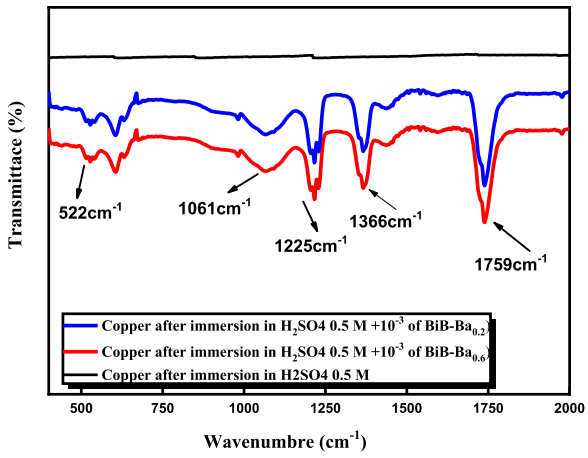

Fig. 18. FTIR spectrum with and without substances of BiB-$Ba_{0.2}$ and BiB-$Ba_{0.6}$ at 10^{-3} M.

Table 9
Inhibition efficiencies for some used inorganic inhibitors in 0.5 M H_2SO_4 solution.

Inorganic inhibitors	Inhibition efficiencies (%)	Ref.
SLS	98	[74]
$Bi_{0.4}Ba_{0.1}P_{0.70}V_{0.70}O_{4.2}$	98.2	[75]
BVP1	91	[76]
Ca^{+}-BDT	91	[77]
BiB-$Ba_{0.2}$	91.2	This work
BiB-$Ba_{0.6}$	90.8	This work

experimental parameters. For the various concentrations, the surface coverage rate (θ) is determined based on the Eq. 10 below[59]

$$\theta = \frac{\eta_{EIS}}{100} = \left(1 - \frac{R_P^{\circ}}{R_P}\right) \quad (10)$$

Various isotherm patterns were plotted to identify the best adsorption model for our inhibitor, using the Eqs. 11–14 following [60,61].

$$\frac{C_{inh}}{\theta} = \frac{1}{K_{ads}} + C_{inh} \quad (11)$$

$$\ln\theta = \ln(K_{ads}) + a\ln(C_{inh}) \quad (12)$$

$$\theta = -\frac{1}{2a}\ln\left(K_{ads}\right) - \frac{1}{2a}\ln\left(C_{inh}\right) \quad (13)$$

$$\ln\left(\frac{\theta}{1-\theta}\right) = \ln\left(K_{ads}\right) + y\ln(C_{inh}) \quad (14)$$

Where y the heterogeneity parameter, a present the term of the lateral interaction, and K_{ads} the equilibrium adsorption constant[62].

The Gibbs free energy (ΔG_{ads}) required to understand the nature of inhibitor adsorption on the Cu surface was calculated according to the following Eq. 15[63].

$$\Delta G_{ads}^{0} = -RT\ln(55.5K_{ads}) \quad (15)$$

Where R stands for the perfect gas constant, T symbolizes the temperature, and the value 55.5 denotes the concentration of water[64].

Table 3 and Fig. 9 present the results of the Langmuir adsorption isotherm model used to describe the adsorption of molecules onto the copper metal surface. The R^2 value is equal to 1, indicating a perfect correlation between the experimental data and the Langmuir isotherm model. Additionally, it can be observed from Fig. 9 that there is a linear relationship between $\ln(C_{inh}/\theta)$ and $\ln(C_{inh})$, indicating that the natural logarithm of the ratio of initial inhibitor concentration to surface coverage ($\ln(C_{inh}/\theta)$) is directly proportional to the natural logarithm of the initial inhibitor concentration ($\ln C_{inh}$). This confirms the validity of the Langmuir isotherm as the best-fitting model for the adsorption process [65].(Table 4)

Table 5 presents the K_{ads} values, indicating a high binding energy between the compounds and the Cu interface. These values suggest a strong affinity for the metal surface, indicating a robust adsorption process. Additionally, Table 5 shows negative ΔG_{ads} values, specifically −45.2 kJ/mol for the sample of BiB-$Ba_{0.2}$ and −45.1 kJ/mol for the sample of BiB-$Ba_{0.6}$, indicating spontaneous adsorption [66]. When ΔG_{ads} is negative, it indicates that the adsorption process is thermodynamically favorable and spontaneous. Negative ΔG_{ads} values also imply a strong interaction between the inhibitor molecules and the Cu surface, indicating that chemisorption is occurring. Chemisorption is a type of adsorption characterized by the formation of chemical bonds [67]. In summary, samples of BiB-$Ba_{0.2}$ and BiB-$Ba_{0.6}$ exhibit high K_{ads} values, negative ΔG_{ads} values, and chemisorption-type adsorption. These observations collectively suggest a stable chemical interaction between the inhibitor molecules and the Cu surface, as well as spontaneous adsorption and a high binding energy [68].

3.3. Temperature effect

The study conducted a potentiodynamic polarization analysis to investigate the impact of temperature variations on the inhibitory performance of all tested inhibitors on the corrosion of Cu surfaces. The PDP curves shown in Fig. 10 were obtained from experiments conducted on both blank samples and samples treated with the two compounds at a concentration of 10^{-3} M. The experiments involved immersing copper samples in a corrosive environment for 30 minutes, with temperatures ranging from 298 to 328 K. Table 6 presents the polarization parameters obtained from the Tafel analysis, providing insights into the corrosion behavior and the effectiveness of the inhibitors under different temperature conditions.

Raising the temperature speeds up both cathodic and anodic reactions, which may cause the detachment of absorbed inhibitors and the rapid dissolution of the metal, resulting in a relative increase in current density. The PDP parameters in Table 6 show that i_{corr} also increases as the temperature rises in a sulfuric acid-rich environment, despite the addition of 10^{-3} M of the studied compounds. However, compounds of BiB-$Ba_{0.2}$ and BiB-$Ba_{0.6}$ reduce i_{corr} cathodically and function as effective anodic inhibitors. It is important to note that the efficacy of these compounds significantly diminishes with an increase in temperature

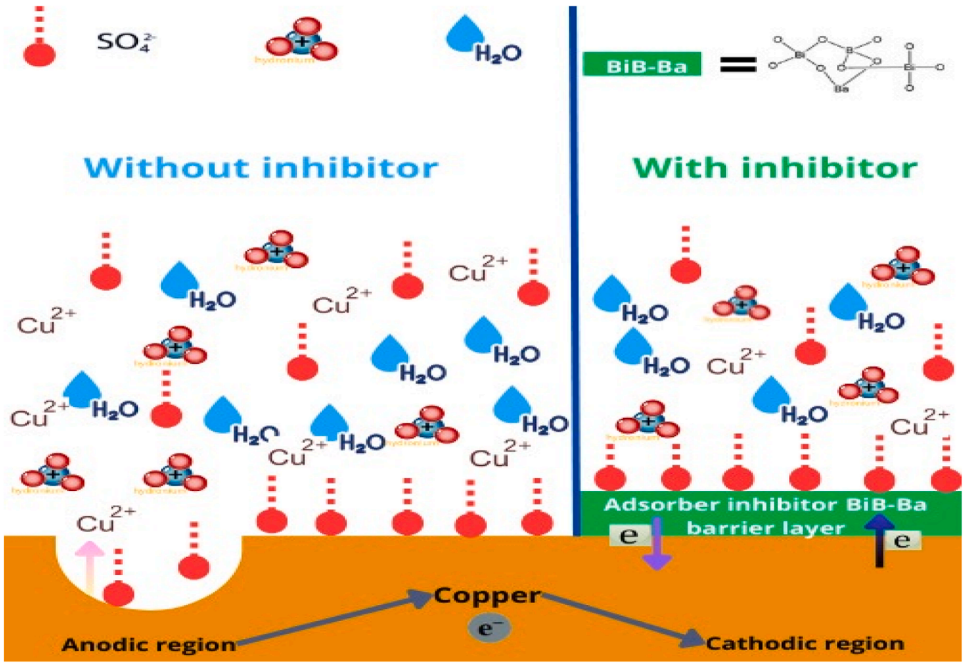

Fig. 19. Schematic representation depicts the adsorption mechanism of the inorganic compounds BiB-Ba and BiB-Ba on the copper surface in a 0.5 M H_2SO_4 solution.

from 298 to 328 K, highlighting their potential significance in inhibiting copper corrosion in harsh environments[9].

3.4. Parameters for activation of the corrosion process

Fig. 11 illustrates the logarithmic variation of i_{corr} with respect to the inverse of temperature (1000/T). This representation demonstrates that the curves adhere to Arrhenius' law when linearized with a slope equal to $-E_a/RT$. The activation energy values have been calculated based on this slope.(Fig. 12)

The data displayed in Table 7 show that the values of *Ea*, *ΔHa*, and *ΔSa* after the addition of two inhibitors BiB-$Ba_{0.2}$ and BiB-$Ba_{0.6}$ at 10^{-3} M are higher than those of the blank solution for copper corrosion. The higher values of Ea with an optimum concentration (10^{-3}) for the two inhibitors can be explained by the formation of a massive protective layer on the copper surface, implying that its adsorption occurs according to the chemisorption mechanism. Furthermore, the increase in E_a can be linked to an expansion of the energy barrier, which is more important for corrosion processes in inhibited environments, suggesting that the layer of adsorbed molecules prevents the charge transfer reaction from occurring at the copper surface and thus protects the metal from dissolution.

The positive ΔHa values for the two inhibitors, BiB-$Ba_{0.2}$ and BiB-$Ba_{0.6}$, are higher than those for the blank solution, as shown in Table 7. These results clearly indicate that the phenomenon of adsorption of inorganic compounds onto the copper substrate in an aggressive environment is endothermic. In addition, the ΔSa values increased negatively after the addition of the inhibitors BiB-$Ba_{0.2}$ and BiB-$Ba_{0.6}$ compared with the blank solution in acidic medium, meaning that turbidity decreases during the transformation of the reagents into an activated complex.

3.5. SEM/EDS characterization

SEM images of copper surfaces treated in a corrosive environment with 0.5 M H_2SO_4 for 12 hours before and after the introduction of substances BiB-$Ba_{0.2}$ and BiB-$Ba_{0.6}$ at a concentration of 10^{-3} M are shown in Fig. 13. These images are intended to demonstrate and quantify the adsorption phenomena occurring between the metal surface and the inorganic substances applied. From Fig. 13 it can be seen that the SEM images show significant degradation and the formation of trace cracks on the surface of the metal immersed in the uninhibited virgin solution. In addition, scratches, voids, and corrosion products were observed on the surface of the copper tested.

Following the addition of the new compounds at a concentration of 10^{-3} M, the metal surface appears smoother, indicating the formation of a protective layer that reduces the damaged and corroded areas of the copper surface. In addition, the images show that the passive film formed at the interface effectively envelops the metal and blocks the active sites.

Fig. 14 illustrates the distribution of chemical elements on the surface of copper before and after the addition of two inhibitors at an optimum concentration of 10^{-3}. The figure confirms the presence of inorganic molecules on the copper substrate and demonstrates the formation of a protective barrier when the tested substances interact with the copper surface in an acidic environment.

The EDS spectra obtained after immersing metallic copper in 0.5 M H_2SO_4 for 12 hours without an inhibitor, as shown in Fig. 15, reveal several possible observations. Firstly, it is evident that the intensity of the copper peak decreases significantly, indicating the dissolution of copper in the acidic solution. Simultaneously, the intensity of the oxygen and sulfur peaks has remarkably increased, indicating the formation of copper oxides and sulfides on the metal surface after exposure to the acidic environment.

The EDS spectra show significant changes when the BiB-$Ba_{0.2}$ and BiB-$Ba_{0.6}$ inhibitors are added to the acid medium. The intensity of the oxygen peak decreases, indicating a reduction in the formation of copper oxides and sulfides. Additionally, new peaks corresponding to the elements Bi, B, and Ba appear. This suggests that inorganic molecules containing bismuth, boron, and barium adsorb onto the copper surface in the presence of these inhibiting substances. In this case, the adsorbed molecules form a protective layer that prevents aggressive ions from attacking the copper's metallic surface. Therefore, the inhibitors effectively protect the copper metal against corrosion, as demonstrated by the alteration of the EDS spectra.

Table 8 displays the atomic percentages of the chemical elements Cu, S, O, Bi, B, and Ba. The results indicate that the percentage of copper increases in the presence of two inhibitors, suggesting the adsorption of

a protective film on the copper surface by molecularly structured heteroatoms. These findings confirm the trend in inhibitory efficacy observed in the electrochemical experimental studies.

3.6. Atomic force microscope observation

The surface of the copper electrode was analyzed using AFM after immersion in an acid medium containing H_2SO_4, both with and without the addition of 10^{-3} M of two inorganic compounds examined at 298 K, as shown in Fig. 15. The exposed surface of the copper electrode displayed several significant fractures and rusts. The copper electrodes' surfaces are flatter and smoother than those of the corroded samples, enabling early analysis of PDP and EIS at concentrations of 10^{-3} M for the two chemical compounds studied. Furthermore, in a medium containing only sulfuric acid, without the examined inorganic compounds, corrosion damage is caused by sulfur ions present in the copper electrode region. Furthermore, when a concentration of 10^{-3} M of the two inorganic molecules BiB-$Ba_{0.2}$ and BiB-$Ba_{0.6}$ is present, they protect the copper ions, resulting in a relatively even distribution within the copper electrodes. The mean roughness of the copper electrode is 311 nm in the absence of inhibitors and 39.03 nm and 38.34 nm in the presence of 10^{-3} M of the inhibitors BiB-$Ba_{0.2}$ and BiB-$Ba_{0.6}$ respectively, in an acidic medium. The surface radius values for the white solution and 10^{-3} M of the inhibitors BiB-$Ba_{0.2}$ and BiB-$Ba_{0.6}$ are 244.11 nm, 35.29 nm, and 55.95 nm, respectively. Furthermore, roughness values below 10^{-3} M of BiB-$Ba_{0.2}$ and BiB-$Ba_{0.6}$ inhibitors indicate that the two inorganic compounds examined safeguard the copper electrode surface in a corrosive environment.

3.7. X-ray diffraction analysis

Fig. 16 displays the XRD diagrams of the corrosion products absorbed by copper after immersion in the corrosive medium for 12 hours. The XRD spectra show three intense and significant diffraction peaks located at 42.4°, 50.9°, and 73.6°, respectively, attributed to the different crystal planes of the Cu (111), Cu (200), and Cu (220) copper networks. The experiment was conducted in the absence and presence of the various substances BiB-$Ba_{0.2}$ and BiB-$Ba_{0.6}$ at 10^{-3} M. The results show a significant increase in the intensity of diffraction peaks for samples exposed to a corrosive environment, especially in the presence of H_2SO_4, both before and after the addition of two inhibiting substances, compared to the pristine sample [69]. This increase in intensity indicates the formation of complex crystalline structures, which suggest interactions between the inhibitors, the copper surface, and the corrosive species. The difference in peak intensity indicates a significant change in the composition and crystalline structure of the corrosion products due to the presence of the corrosive environment and inhibitors [70]. Furthermore, the XRD spectrum of the blank sample revealed a distinct Cu_2O peak at 37.2°, indicating the formation of copper oxide (Cu_2O) as one of the corrosion products in the presence of the corrosive environment [71].(Fig. 17)

In contrast, when the two inhibitors BiB-$Ba_{0.2}$ and BiB-$Ba_{0.6}$ were added at a concentration of 10^{-3} M, the synthesis of these oxides was significantly slowed down. This was evidenced by the absence of a comparable diffraction peak in the XRD spectrum after their addition. It is believed that the delay is due to the formation of a barrier that protects the metal surface from the corrosive effects of the virgin solution.

3.8. FTIR characterization

In this study, FTIR was utilized as a powerful analytical tool to investigate the molecular composition of compounds adsorbed onto the copper surface before and after treatment. The FTIR spectra obtained from the samples immersed in the corrosive medium for 12 hours, both in the absence and presence of the inhibitors BiB-$Ba_{0.2}$ and BiB-$Ba_{0.6}$ at a concentration of 10^{-3} M, were examined as shown in Fig. 18. Upon analyzing the FTIR spectra, a significant distinction was observed between the blank sample and the samples treated with inhibitors. In the FTIR spectra of the blank sample, the absence of peaks corresponding to the studied products was evident. This absence indicates that, in the absence of inhibiting substances, specific molecules did not adsorb onto the copper surface or form any discernible protective film [72]. Conversely, when the inhibitors BiB-$Ba_{0.2}$ and BiB-$Ba_{0.6}$ were introduced into the corrosive medium, substantial changes were noted in the FTIR spectra. These changes were characterized by the presence of several distinct peaks corresponding to the molecules under investigation. The emergence of these peaks strongly suggests that the inorganic compounds studied successfully adsorbed onto the copper substrate, forming a protective film [73]. The formation of this protective film on the copper substrate is crucial in preventing further corrosion, as it acts as a barrier, hindering the interaction between the corrosive environment and the underlying metal.

3.9. Comparative corrosion inhibition performance

The comparative corrosion inhibitory efficiency of the inorganic inhibitor in 0.5 M H_2SO_4 solution with others inhibitors are displayed in Table 9. The corrosion efficiencies values, found through EIS measurements are compared with other inorganic inhibitors previously investigated and used in the same conditions. Table 9 illustrated that the two inorganic inhibitors investigated in this work exhibits a similar inhibitory efficiency that other inorganic inhibitors.

3.10. Mechanism of inhibition

Fig. 19 illustrates a corrosion protection scheme for copper immersed in a 0.5 M sulfuric acid solution utilizing glass. The adsorption of inorganic molecules on the metal surface impedes the dissolution process by preventing anodic and cathodic reactions, or both. This corrosion protection framework is derived from a synthesis of experimental results. The results of the electrochemical tests demonstrate that cathodic and anodic reactions occur at the surface of the copper electrode. It is proposed that bismuth (Bi) and barium, present in borate glass, form an insoluble layer of $Bi(OH)_3$ and $Ba(OH)_2$ [78,79]. Furthermore, the heteroatoms of B, in addition to oxygen and borate groups with their free electrons, are capable of reacting with Cu ions to form a film on the surface, thereby slowing down the dissolution process of the metal. Consequently, inorganic molecules are capable of forming coordination bonds with cuprous ions, thereby enabling their adsorption onto the copper/solution interface. This results in the formation of a stable barrier film that effectively inhibits the anodic and cathodic reactions of copper in the H_2SO_4 medium. The corrosion inhibition efficiency of the inhibitor in 0.5 M H_2SO_4 can be explained by factors such as the number of adsorption sites, charge density, molecular size, mode of interaction with the metal surface, and ability to form metal complexes.

4. Conclusion

The objective of this research was to investigate the behavior, inhibition efficacy, and corrosion mechanism of inorganic corrosion inhibitors on copper-based metals in a corrosive medium containing 0.5 M H_2SO_4 solution. Electrochemical and morphological studies were conducted to analyze the copper substrates used in the corrosion tests. PDP and EIS tests showed that both inhibitors had high inhibitory efficiencies at the optimum concentration (10^{-3} M). BiB-$Ba_{0.2}$ inhibitor had an efficiency of 91.2 %, while the BiB-$Ba_{0.6}$ inhibitor had an efficiency of 90.8 %. The results obtained by the PDP and EIS techniques suggest that the inorganic compounds investigated can be strongly adsorb onto copper substrates, acting as mixed-type corrosion inhibitors. XRD, FTIR, SEM/EDS, and AFM analyzes techniques used in this study suggest that the two inhibitors added to the corrosive medium adsorb onto the copper surface, forming a protective layer that reduces damage and

corrosion of the metal.

CRediT authorship contribution statement

Rachid Hsissou: Writing – original draft, Investigation. **Basheer M. Al-Maswari:** Visualization, Validation. **Marouane El-alouani:** Data curation. **Zaroual Aziz:** Formal analysis. **Issam saber:** Writing – review & editing, Writing – original draft. **M.S. El youbi:** Validation. **khadija dahmani:** Writing – original draft. **mouhsine galai:** Validation, Supervision. **Mohamed Ebn Touhami:** Validation, Supervision. **Soumya Ferraa:** Software. **Nouf H. Alotaibi:** Supervision. **Otmane Kharbouch:** Writing – original draft. **Zakia Aribou:** Software, Methodology.

Declaration of Competing Interest

The authors declare that they have no known competing financial interests or personal relationships that could have appeared to influence the work reported in this paper.

Acknowledgment

This work was funded by the Researchers Supporting Project Number (RSPD2024R551) King Saud University, Riyadh, Saudi Arabia.

References

[1] R. Hsissou, K. Dahmani, A. El Magri, A. Hmada, Z. Safi, N. Dkhireche, M. Galai, N. Wazzan, A. Berisha, A combined experimental and computational (DFT, RDF, MC and MD) investigation of epoxy resin as a potential corrosion inhibitor for mild steel in a 0.5 M H2SO4 environment, Polymers 15 (2023), https://doi.org/10.3390/polym15081967.

[2] A. Ech-chebab, M. Missioui, L. Guo, O. El Khouja, R. Lachhab, O. Kharbouch, M. Galai, M. Ouakki, A. Ejbouh, K. Dahmani, N. Dkhireche, M. Ebn Touhami, Evaluation of quinoxaline-2(1H)-one, derivatives as corrosion inhibitors for mild steel in 1.0 M acidic media: electrochemistry, quantum calculations, dynamic simulations, and surface analysis, Chem. Phys. Lett. 809 (2022) 140156, https://doi.org/10.1016/J.CPLETT.2022.140156.

[3] K. Dahmani, M. Galai, M. Ouakki, A. Elgendy, R. Ez-Zriouli, R. Lachhab, S. Briche, M. Cherkaoui, Corrosion inhibition of copper in sulfuric acid via environmentally friendly inhibitor (Myrtus communis): combining experimental and theoretical methods, J. Mol. Liq. 347 (2022) 117982, https://doi.org/10.1016/j.molliq.2021.117982.

[4] B. Tan, S. Zhang, Y. Qiang, L. Feng, C. Liao, Y. Xu, S. Chen, Investigation of the inhibition effect of Montelukast Sodium on the copper corrosion in 0.5 mol/L H2SO4, J. Mol. Liq. 248 (2017) 902–910, https://doi.org/10.1016/j.molliq.2017.10.111.

[5] Z. Aribou, M. Ouakki, N. Khemmou, S. Sibous, E. Ech-chihbi, O. Kharbouch, M. Galai, A. Souizi, S. Boukhris, M.E. Touhami, A.A. AlObaid, I. Warad, Exploring the adsorption and corrosion inhibition properties of indazole as a corrosion inhibitor for brass alloy in HCl medium: a theoretical and experimental study, Mater. Today Commun. 37 (2023) 107061, https://doi.org/10.1016/j.mtcomm.2023.107061.

[6] Z. El-kiri, A. Hmada, R. Sayed, K. Dakhsi, A. Larioui, F. Benhiba, R. Hsissou, N. Dkhireche, M. Galai, M. EbnTouhami, Correlation between experimental and theoretical approaches in the performance of new epoxy resin as an effective corrosion inhibitor for mild steel in acid pickling bath, J. Mol. Struct. 1294 (2023) 136466, https://doi.org/10.1016/j.molstruc.2023.136466.

[7] K. Mzioud, A. Habsaoui, M. Ouakki, M. Galai, S. El Fartah, M. Ebn Touhami, Inhibition of copper corrosion by the essential oil of Allium sativum in 0.5M H2SO4 solutions, SN Appl. Sci. 2 (2020) 1–13, https://doi.org/10.1007/s42452-020-03393-8.

[8] B. Tan, S. Zhang, Y. Qiang, L. Guo, L. Feng, C. Liao, Y. Xu, S. Chen, A combined experimental and theoretical study of the inhibition effect of three disulfide-based flavouring agents for copper corrosion in 0.5 M sulfuric acid, J. Colloid Interface Sci. 526 (2018) 268–280, https://doi.org/10.1016/j.jcis.2018.04.092.

[9] Y. Qiang, S. Zhang, H. Zhao, B. Tan, L. Wang, Enhanced anticorrosion performance of copper by novel N-doped carbon dots, Corros. Sci. 161 (2019) 108193, https://doi.org/10.1016/j.corsci.2019.108193.

[10] C. Xu, W. Li, B. Tan, X. Zuo, S. Zhang, Adsorption of Gardenia jasminoides fruits extract on the interface of Cu/H2SO4 to inhibit Cu corrosion: experimental and theoretical studies, J. Mol. Liq. 345 (2022) 116996, https://doi.org/10.1016/j.molliq.2021.116996.

[11] H. Li, S. Zhang, B. Tan, Y. Qiang, W. Li, S. Chen, L. Guo, Investigation of Losartan Potassium as an eco-friendly corrosion inhibitor for copper in 0.5 M H2SO4, J. Mol. Liq. 305 (2020) 112789, https://doi.org/10.1016/j.molliq.2020.112789.

[12] J. Chen, Y. Qiang, S. Peng, Z. Gong, S. Zhang, L. Gao, B. Tan, S. Chen, L. Guo, Experimental and computational investigations of 2-amino-6-bromobenzothiazole as a corrosion inhibitor for copper in sulfuric acid, J. Adhes. Sci. Technol. 32 (2018) 2083–2098, https://doi.org/10.1080/01694243.2018.1460948.

[13] S. Rached, A. Habsaoui, K. Mzioud, R. Lachhab, S. Haida, N. Errahmany, M. Galai, M.E. Touhami, Valorization of the green corrosion inhibitor Marrubium vulgare L.: electrochemical, thermodynamic, theoretical & surface studies, Chem. Data Collect. 48 (2023) 101099, https://doi.org/10.1016/j.cdc.2023.101099.

[14] R. Hsissou, B. Benzidia, N. Hajjaji, A. Elharfi, ELABORATION AND ELECTROCHEMICAL STUDIES OF THE COATING BEHAVIOR OF A NEW PENTAFUNCTIONAL EPOXY POLYMER (PENTAGLYCIDYL ETHER PENTABISPHENOL PHOSPHORUS) ON E24 CARBON STEEL IN 3.5% NaCl, 2018.

[15] F. Benhiba, R. Hsissou, K. Abderrahim, H. Serrar, Z. Rouifi, S. Boukhris, G. Kaichouh, A. Bellaouchou, A. Guenbour, H. Oudda, I. Warad, A. Zarrouk, Development of new pyrimidine derivative inhibitor for mild steel corrosion in acid medium, J. Biol. Tribocorros 8 (2022) 36, https://doi.org/10.1007/s40735-022-00637-5.

[16] L. Feng, S. Zhang, Y. Lu, B. Tan, S. Chen, L. Guo, Synergistic corrosion inhibition effect of thiazolyl-based ionic liquids between anions and cations for copper in HCl solution, Appl. Surf. Sci. 483 (2019) 901–911, https://doi.org/10.1016/j.apsusc.2019.03.299.

[17] K. Dahmani, M. Galai, M. Ouakki, M. Cherkaoui, R. Touir, S. Erkan, S. Kaya, B. El Ibrahimi, Quantum chemical and molecular dynamic simulation studies for the identification of the extracted cinnamon essential oil constituent responsible for copper corrosion inhibition in acidified 3.0 wt% NaCl medium, Inorg. Chem. Commun. 124 (2021), https://doi.org/10.1016/j.inoche.2020.108409.

[18] X. Guo, H. Huang, D. Liu, The inhibition mechanism and adsorption behavior of three purine derivatives on the corrosion of copper in alkaline artificial seawater: structure and performance, Colloids Surf. A Physicochem Eng. Asp. 622 (2021) 126644, https://doi.org/10.1016/j.colsurfa.2021.126644.

[19] Z.G. Luo, Y. Zhang, H. Wang, S. Wan, L.F. Song, B.K. Liao, X.P. Guo, Modified nano-lignin as a novel biomass-derived corrosion inhibitor for enhanced corrosion resistance of carbon steel, Corros. Sci. 227 (2024), https://doi.org/10.1016/j.corsci.2023.111705.

[20] S.Q. Ma, H.L. Huang, S. Wan, L. Hao, B.K. Liao, X.P. Guo, Experimental, theoretical and computational studies of oxalyl dihydrazide as a novel corrosion inhibitor for mild steel in neutral saline solution, Colloids Surf. A Physicochem Eng. Asp. 699 (2024), https://doi.org/10.1016/j.colsurfa.2024.134717.

[21] J. Zhang, L. Zhang, G. Tao, A novel and high-efficiency inhibitor of 5-(4-methoxyphenyl)-3h-1,2-dithiole-3-thione for copper corrosion inhibition in sulfuric acid at different temperatures, J. Mol. Liq. 272 (2018) 369–379, https://doi.org/10.1016/j.molliq.2018.09.095.

[22] G. Ghenimi, M. Ouakki, H. Barebita, A.El Fazazi, T. Guedira, M. Cherkaoui, New Vitreous Phase as Mild Steel Inhibitors in Hydrochloric Acid, 2020. ⟨www.abechem.com⟩.

[23] R. Hsissou, A. El Magri, E. Ech-chihbi, A. Hmada, I. Saber, A. Berisha, N. Dkhireche, D. Ouzebla, M. Rbaa, F. Benhiba, L. Khamliche, M. Daoudi, Elaboration and investigation of formulated polymer composites as some potential anticorrosion coatings for brass surface in 3.5% NaCl solution: theoretical approaches, Canadian Metallurgical Quarterly (n.d.) 1–18. https://doi.org/10.1080/00084433.2024.2399872.

[24] B. Baach, M. Ouakki, S. Ferraa, H. Barebita, M. Cherkaoui, A. Nimour, T. Guedira, Experimental evaluation of new inorganic compounds based on bismuth oxide Bi2O3 as corrosion inhibition for mild steel in acidic medium, Inorg. Chem. Commun. 137 (2022) 109233, https://doi.org/10.1016/j.inoche.2022.109233.

[25] K. Ba, A. Chahine, M. Ebn Touhami, J.G. Alauzun, A. Manseri, Preparation and characterization of phosphate-nickel-titanium composite coatings obtained by sol–gel process for corrosion protection, SN Appl. Sci. 2 (2020) 1–13, https://doi.org/10.1007/s42452-020-2173-x.

[26] O. Dagdag, R. Hsissou, A. El Harfi, L. El Gana, Z. Safi, L. Guo, C. Verma, E. E. Ebenso, M. El Gouri, Development and anti-corrosion performance of polymeric epoxy resin and their zinc phosphate composite on 15CDV6 steel in 3wt% NaCl: experimental and computational studies, J. Biol. Tribocorros 6 (2020) 112, https://doi.org/10.1007/s40735-020-00407-1.

[27] M. Damej, A. Molhi, H. Lgaz, R. Hsissou, J. Aslam, M. Benmessaoud, N. Rezki, H.-S. Lee, D.-E. Lee, Performance and interaction mechanism of a new highly efficient benzimidazole-based epoxy resin for corrosion inhibition of carbon steel in HCl: a study based on experimental and first-principles DFTB simulations, J. Mol. Struct. 1273 (2023) 134232, https://doi.org/10.1016/j.molstruc.2022.134232.

[28] A. El Magri, R. Hsissou, A. Hmada, A. Berisha, N. Dkhireche, S. Vaudreuil, Development of new polymer composites formulated by glass as a potential protective coating for 3D printed H13 steel in acidic medium: DFT, MC and MD computational, J. Mol. Liq. 387 (2023) 122690, https://doi.org/10.1016/j.molliq.2023.122690.

[29] A. Elbadaoui, M. Galai, S. Ferraa, H. Barebita, M. Cherkaoui, T. Guedira, A New Family of Borated Glasses as a Corrosion Inhibitor for Carbon Steel in Acidic Medium (1.0 M HCl), 2019. ⟨www.abechem.com⟩.

[30] S. Ferraa, M. Ouakki, H. Barebita, A. Nimour, M. Cherkaoui, T. Guedira, Corrosion inhibition potentials of some phosphovanadate-based glasses on mild steel in 1 M HCl, Inorg. Chem. Commun. 132 (2021) 108806, https://doi.org/10.1016/j.inoche.2021.108806.

[31] I. Saber, K. Dahmani, M. Galai, A. EL Magri, R. Hsissou, H. Barbita, M. Belfaquir, I. Warad, N. AL-Zaqri, M.S. Elyoubi, Synthesis and characterization of new eco-friendly vitreous system Bi2O3–B2O3–BaO: structural, morphologic, and thermal analysis, Opt. Mater. (Amst.) 149 (2024) 115079, https://doi.org/10.1016/j.optmat.2024.115079.

[32] L. Haritha, K. Chandra Sekhar, R. Nagaraju, G. Ramadevudu, V.G. Sathe, M. Shareefuddin, Effect of metal fluorides on chromium ions doped bismuth borate

glasses for optical applications, Chin. Phys. B 28 (2019), https://doi.org/10.1088/1674-1056/28/3/038101.
[33] R.S. Kundu, S. Dhankhar, R. Punia, K. Nanda, N. Kishore, Bismuth modified physical, structural and optical properties of mid-IR transparent zinc boro-tellurite glasses, J. Alloy. Compd. 587 (2014) 66–73, https://doi.org/10.1016/j.jallcom.2013.10.141.
[34] C. Gautam, A.K. Yadav, V.K. Mishra, K. Vikram, Synthesis, IR and Raman spectroscopic studies of (Ba,Sr)TiO₃ borosilicate glasses with addition of La₂O<sub>3</sub&gt, Open J. Inorg. Non-Met. Mater. 02 (2012) 47–54, https://doi.org/10.4236/ojinm.2012.24005.
[35] A.V. Egorysheva, V.D. Volodin, V.M. Skorikov, Glass formation in the Bi 2O 3-B 2O 3-BaO system, Inorg. Mater. 44 (2008) 1261–1265, https://doi.org/10.1134/S0020168508110228.
[36] H. Doweidar, Y.B. Saddeek, FTIR and ultrasonic investigations on modified bismuth borate glasses, J. Non Cryst. Solids 355 (2009) 348–354, https://doi.org/10.1016/j.jnoncrysol.2008.12.008.
[37] E. Mansour, FTIR spectra of pseudo-binary sodium borate glasses containing TeO 2, J. Mol. Struct. 1014 (2012) 1–6, https://doi.org/10.1016/j.molstruc.2012.01.034.
[38] M. Galai, K. Dahmani, M. Ebn Touhami, R. Hsissou, F. Benhiba, M. Rbaa, M. Ouakki, R. Lachhab, S.M. AlharbiCorrosion inhibition of brass electrode in 3% NaCl medium using novel quinoline derivatives based on D-glucose: Synthesis, characterization, and mechanistic insights through experimental and computational approaches, Materials Science and Engineering: B 298 (2023). https://doi.org/10.1016/j.mseb.2023.116843 .
[39] R. Hsissou, A. El Magri, E. Ech-chihbi, A. Hmada, I. Saber, A. Berisha, N. Dkhireche, D. Ouzebla, M. Rbaa, F. Benhiba, L. Khamliche, M. Daoudi, Elaboration and investigation of formulated polymer composites as some potential anticorrosion coatings for brass surface in 3.5% NaCl solution: theoretical approaches, Canadian Metallurgical Quarterly (n.d.) 1–18. https://doi.org/10.1080/00084433.2024.2399872.
[40] K. Dahmani, M. Galai, M. Rbaa, A. Ech-Chebab, N. Errahmany, L. Guo, A. A. AlObaid, A. Hmada, I. Warad, B. lakhrissi, M. Ebn Touhami, M. Cherkaoui, Evaluating the efficacy of synthesized quinoline derivatives as Corrosion inhibitors for mild steel in acidic environments: an analysis using electrochemical, computational, and surface techniques, J. Mol. Struct. 1295 (2024) 136514, https://doi.org/10.1016/j.molstruc.2023.136514.
[41] A. Palit, S.O. Pehkonen, Copper corrosion in distribution systems: evaluation of a homogeneous Cu2O film and a natural corrosion scale as corrosion inhibitors, Corros. Sci. 42 (2000) 1801–1822, https://doi.org/10.1016/S0010-938X(00)00024-X.
[42] L. Guo, B. Tan, X. Zuo, W. Li, S. Leng, X. Zheng, Eco-friendly food spice 2-Fur-furylthio-3-methylpyrazine as an excellent inhibitor for copper corrosion in sulfuric acid medium, J. Mol. Liq. 317 (2020) 113915, https://doi.org/10.1016/j.molliq.2020.113915.
[43] Y. Qiang, L. Guo, H. Li, X. Lan, Fabrication of environmentally friendly Losartan potassium film for corrosion inhibition of mild steel in HCl medium, Chem. Eng. J. 406 (2021) 126863, https://doi.org/10.1016/j.cej.2020.126863.
[44] L. Feng, S. Zhang, Y. Qiang, Y. Xu, L. Guo, L.H. Madkour, S. Chen, Experimental and theoretical investigation of thiazolyl blue as a corrosion inhibitor for copper in neutral sodium chloride solution, Materials 11 (2018), https://doi.org/10.3390/ma11061042.
[45] Z.Z. Tasic, M.M. Antonijevic, M.B. Petrovic Mihajlovic, M.B. Radovanovic, The influence of synergistic effects of 5-methyl-1H-benzotriazole and potassium sorbate as well as 5-methyl-1H-benzotriazole and gelatin on the copper corrosion in sulphuric acid solution, J. Mol. Liq. 219 (2016) 463–473, https://doi.org/10.1016/j.molliq.2016.03.064.
[46] Z. Xu, Y. Gan, J. Zeng, J. Chen, A. Fu, X. Zheng, W. Li, Green synthesis of functionalized fluorescent carbon dots from biomass and their corrosion inhibition mechanism for copper in sulfuric acid environment, Chem. Eng. J. 470 (2023) 144425, https://doi.org/10.1016/j.cej.2023.144425.
[47] K. Dahmani, M. Galai, A. Ech-Chebab, N. Al-Zaqri, M. Ouakki, A. Elgendy, R. Ez-Zriouli, S.-C. Kim, M.E. Touhami, M. Cherkaoui, Investigating the inhibitory properties of cupressus sempervirens extract against copper corrosion in 0.5 M H 2 SO 4: combining quantum (Density Functional Theory Calculation–Monte Carlo Simulation) and electrochemical-surface studies, ACS Omega (2023), https://doi.org/10.1021/acsomega.3c00589.
[48] Y. Xu, S. Zhang, W. Li, L. Guo, S. Xu, L. Feng, L.H. Madkour, Experimental and theoretical investigations of some pyrazolo-pyrimidine derivatives as corrosion inhibitors on copper in sulfuric acid solution, Appl. Surf. Sci. 459 (2018) 612–620, https://doi.org/10.1016/j.apsusc.2018.08.037.
[49] H. Huang, F. Bu, Correlations between the inhibition performances and the inhibitor structures of some azoles on the galvanic corrosion of copper coupled with silver in artificial seawater, Corros. Sci. 165 (2020) 108413, https://doi.org/10.1016/j.corsci.2019.108413.
[50] Y. Zhang, B. Tan, X. Zhang, L. Guo, S. Zhang, Synthesized carbon dots with high N and S content as excellent corrosion inhibitors for copper in sulfuric acid solution, J. Mol. Liq. 338 (2021) 116702, https://doi.org/10.1016/j.molliq.2021.116702.
[51] B. Tan, W. Lan, S. Zhang, H. Deng, Y. Qiang, A. Fu, Y. Ran, J. Xiong, R. Marzouki, W. Li, Passiflora edulia Sims leaves Extract as renewable and degradable inhibitor for copper in sulfuric acid solution, Colloids Surf. A Physicochem Eng. Asp. 645 (2022) 128892, https://doi.org/10.1016/j.colsurfa.2022.128892.
[52] M.M. Solomon, S.A. Umoren, A. Gilda Ritacca, I. Ritacco, D. Hu, L. Guo, Tailoring poly(2-ethyl-2-oxazoline) towards effective mitigation of chloride-induced dissolution of S235JR steel: the synergistic contributions of potassium iodide and myristyl trimethylammonium bromide, J. Mol. Liq. 396 (2024) 123935, https://doi.org/10.1016/j.molliq.2023.123935.
[53] A. Belakhdar, H. Ferkous, S. Djellali, R. Sahraoui, H. Lahbib, Y.Ben Amor, A. Erto, M. Balsamo, Y. Benguerba, Computational and experimental studies on the efficiency of Rosmarinus officinalis polyphenols as green corrosion inhibitors for XC48 steel in acidic medium, Colloids Surf. A Physicochem Eng. Asp. 606 (2020) 125458, https://doi.org/10.1016/j.colsurfa.2020.125458.
[54] B. Tan, B. Xiang, S. Zhang, Y. Qiang, L. Xu, S. Chen, J. He, Papaya leaves extract as a novel eco-friendly corrosion inhibitor for Cu in H2SO4 medium, J. Colloid Interface Sci. 582 (2021) 918–931, https://doi.org/10.1016/j.jcis.2020.08.093.
[55] A. Molhi, R. Hsissou, M. Damej, A. Berisha, M. Bamaarouf, M. Seydou, M. Benmessaoud, S.El Hajjaji, Performance of two epoxy compounds against corrosion of C38 steel in 1 M HCl: electrochemical, thermodynamic and theoretical assessment, Int. J. Corros. Scale Inhib. 10 (2021) 812–837, https://doi.org/10.17675/2305-6894-2021-10-2-21.
[56] M. Rehioui, M. Barbouchi, S. Abbout, B. Benzidia, S. Moussaoui, S. Bikri, R. Hsissou, H. Hammouch, H. Erramli, N. Hajjaji, Development of a promising nontoxic corrosion inhibitor based on Opuntia dillenii seed oil for iron corrosion in 3wt% NaCl: experimental and theoretical approaches, Chem. Data Collect. 46 (2023) 101037, https://doi.org/10.1016/j.cdc.2023.101037.
[57] Y. Zhang, S. Zhang, B. Tan, L. Guo, H. Li, Solvothermal synthesis of functionalized carbon dots from amino acid as an eco-friendly corrosion inhibitor for copper in sulfuric acid solution, J. Colloid Interface Sci. 604 (2021) 1–14, https://doi.org/10.1016/j.jcis.2021.07.034.
[58] B. Tan, S. Zhang, H. Liu, Y. Guo, Y. Qiang, W. Li, L. Guo, C. Xu, S. Chen, Corrosion inhibition of X65 steel in sulfuric acid by two food flavorants 2-isobutylthiazole and 1-(1,3-Thiazol-2-yl) ethanone as the green environmental corrosion inhibitors: combination of experimental and theoretical researches, J. Colloid Interface Sci. 538 (2019) 519–529, https://doi.org/10.1016/j.jcis.2018.12.020.
[59] Z. Aribou, M. Ouakki, F. El Hajri, E. Ech-chihbi, I. Saber, Z. Benzekri, S. Boukhris, M.K. Al-Sadoon, M. Galai, J. Charafeddine, M.E. Touhami, Comprehensive assessment of the corrosion inhibition properties of quinazoline derivatives on mild steel in 1.0 M HCl solution: an electrochemical, surface analysis, and computational study, Int J. Electrochem Sci. 19 (2024) 100788, https://doi.org/10.1016/j.ijoes.2024.100788.
[60] B. Tan, S. Zhang, X. Cao, A. Fu, L. Guo, R. Marzouki, W. Li, Insight into the anti-corrosion performance of two food flavors as eco-friendly and ultra-high performance inhibitors for copper in sulfuric acid medium, J. Colloid Interface Sci. 609 (2022) 838–851, https://doi.org/10.1016/j.jcis.2021.11.085.
[61] E. Ech-chihbi, M. Adardour, W. Ettahiri, R. Salim, M. Ouakki, M. Galai, A. Baouid, M. Taleb, Surface interactions and improved corrosion resistance of mild steel by addition of new triazolyl-benzimidazolone derivatives in acidic environment, J. Mol. Liq. 387 (2023) 122652, https://doi.org/10.1016/j.molliq.2023.122652.
[62] E. Alibakhshi, M. Ramezanzadeh, G. Bahlakeh, B. Ramezanzadeh, M. Mahdavian, M. Motamedi, Glycyrrhiza glabra leaves extract as a green corrosion inhibitor for mild steel in 1 M hydrochloric acid solution: experimental, molecular dynamics, Monte Carlo and quantum mechanics study, J. Mol. Liq. 255 (2018) 185–198, https://doi.org/10.1016/j.molliq.2018.01.144.
[63] A. Singh, K.R. Ansari, P. Bedi, T. Pramanik, I.H. Ali, Y. Lin, P. Banerjee, S. Zamindar, Understanding xanthone derivatives as novel and efficient corrosion inhibitors for P110 steel in acidizing fluid: experimental and theoretical studies, J. Phys. Chem. Solids 172 (2023) 111064, https://doi.org/10.1016/j.jpcs.2022.111064.
[64] H. Lgaz, I.M. Chung, M.R. Albayati, A. Chaouiki, R. Salghi, S.K. Mohamed, Improved corrosion resistance of mild steel in acidic solution by hydrazone derivatives: an experimental and computational study, Arab. J. Chem. 13 (2020) 2934–2954, https://doi.org/10.1016/j.arabjc.2018.08.004.
[65] Y. Qiang, S. Zhang, L. Guo, X. Zheng, B. Xiang, S. Chen, Experimental and theoretical studies of four allyl imidazolium-based ionic liquids as green inhibitors for copper corrosion in sulfuric acid, Corros. Sci. 119 (2017) 68–78, https://doi.org/10.1016/j.corsci.2017.02.021.
[66] F. Benhiba, N.K. Sebbar, H. Bourazmi, M.E. Belghiti, R. Hsissou, T. Hökelek, A. Bellaouchou, A. Guenbour, I. Warad, H. Oudda, A. Zarrouk, E.M. Essassi, Corrosion inhibition performance of 4-(prop-2-ynyl)- [1,4]-benzothiazin-3-one against mild steel in 1 M HCl solution: experimental and theoretical studies, Int. J. Hydrog. Energy 46 (2021) 25800–25818, https://doi.org/10.1016/j.ijhydene.2021.05.091.
[67] M. Galai, K. Dahmani, O. Kharbouch, M. Rbaa, N. Alzeqri, L. Guo, A.A. AlObaid, A. Hmada, N. Dkhireche, E. Ech-chihbi, M. Ouakki, M.E. Touhami, I. Warad, Surface analysis and interface properties of a newly synthesized quinoline-derivative corrosion inhibitor for mild steel in acid pickling bath: mechanistic exploration through electrochemical, XPS, AFM, contact angle, SEM/EDS, and computational studies, J. Phys. Chem. Solids 184 (2024) 111681, https://doi.org/10.1016/j.jpcs.2023.111681.
[68] D.K. Verma, E.E. Ebenso, M.A. Quraishi, C. Verma, Gravimetric, electrochemical surface and density functional theory study of acetohydroxamic and benzohydroxamic acids as corrosion inhibitors for copper in 1 M HCl, Results Phys. 13 (2019), https://doi.org/10.1016/j.rinp.2019.102194.
[69] H. Wang, J. Yu, Y. Wu, W. Shao, X. Xu, A facile two-step approach to prepare superhydrophobic surfaces on copper substrates, J. Mater. Chem. A Mater. 2 (2014) 5010–5017, https://doi.org/10.1039/c3ta15102f.
[70] Y. Shi, J. Zhao, L. Chen, H. Li, S. Zhang, F. Gao, Double open mouse-like terpyridine parts based amphiphilic ionic molecules displaying strengthened chemical adsorption for anticorrosion of copper in sulfuric acid solution, Chin. J. Chem. Eng. 57 (2023) 233–246, https://doi.org/10.1016/j.cjche.2022.08.013.
[71] F. Xiao, S. Yuan, B. Liang, G. Li, S.O. Pehkonen, T. Zhang, Superhydrophobic CuO nanoneedle-covered copper surfaces for anticorrosion, J. Mater. Chem. A Mater. 3 (2015) 4374–4388, https://doi.org/10.1039/c4ta05730a.

[72] Y. Zhang, S. Zhang, B. Tan, L. Guo, H. Li, Solvothermal synthesis of functionalized carbon dots from amino acid as an eco-friendly corrosion inhibitor for copper in sulfuric acid solution, J. Colloid Interface Sci. 604 (2021) 1–14, https://doi.org/10.1016/j.jcis.2021.07.034.
[73] W. Zeng, B. Tan, X. Zheng, X. Chen, J. Chen, W. Li, Penetration into the inhibition performance of two piperazine derivatives as high-efficiency inhibitors for copper in sulfuric acid environment, J. Mol. Liq. 356 (2022) 119015, https://doi.org/10.1016/j.molliq.2022.119015.
[74] B.-K. Liao, R.-X. Quan, P.-X. Feng, H. Wang, W. Wang, L. Niu, Carbon steel anticorrosion performance and mechanism of sodium lignosulfonate, Rare Met. 43 (2024) 356–365, https://doi.org/10.1007/s12598-023-02404-y.
[75] S. Ferraa, M. Ouakki, H. Barebita, A. Nimour, M. Cherkaoui, T. Guedira, Corrosion inhibition potentials of some phosphovanadate-based glasses on mild steel in 1 M HCl, Inorg. Chem. Commun. 132 (2021) 108806, https://doi.org/10.1016/j.inoche.2021.108806.
[76] A. Majjane, D. Rair, A. Chahine, M. Et-tabirou, M. Ebn Touhami, R. Touir, Preparation and characterization of a new glass system inhibitor for mild steel corrosion in hydrochloric solution, Corros. Sci. 60 (2012) 98–103, https://doi.org/10.1016/j.corsci.2012.04.006.
[77] A.A. Aghzzaf, B. Rhouta, E. Rocca, A. Khalil, J. Steinmetz, Corrosion inhibition of zinc by calcium exchanged beidellite clay mineral: a new smart corrosion inhibitor, Corros. Sci. 80 (2014) 46–52, https://doi.org/10.1016/j.corsci.2013.10.037.
[78] M. Boudalia, M. Laourayed, M. El Moudane, Z. Sekkat, O.S. Campos, A. Bellaouchou, A. Guenbour, A. José Garcia, H.M.A. Amin, Phosphate glass doped with niobium and bismuth oxides as an eco-friendly corrosion protection matrix of iron steel in HCl medium: experimental and theoretical insights, J. Alloy. Compd. 938 (2023), https://doi.org/10.1016/j.jallcom.2022.168570.
[79] A. Elbadaoui, M. Galai, S. Ferraa, H. Barebita, M. Cherkaoui, T. Guedira, A New Family of Borated Glasses as a Corrosion Inhibitor for Carbon Steel in Acidic Medium (1.0 M HCl), 2019. ⟨www.abechem.com⟩.